DOT/FAA/AR-05/21

Office of Aviation Research
Washington, D.C. 20591

Handling Qualities and Flight Safety Implications of Rudder Control Strategies and Systems in Transport Aircraft

June 2005

Final Report

This document is available to the U.S. public through the National Technical Information Service (NTIS), Springfield, Virginia 22161.

U.S. Department of Transportation
Federal Aviation Administration

NOTICE

This document is disseminated under the sponsorship of the U.S. Department of Transportation in the interest of information exchange. The United States Government assumes no liability for the contents or use thereof. The United States Government does not endorse products or manufacturers. Trade or manufacturer's names appear herein solely because they are considered essential to the objective of this report. This document does not constitute FAA certification policy. Consult your local FAA aircraft certification office as to its use.

This report is available at the Federal Aviation Administration William J. Hughes Technical Center's Full-Text Technical Reports page: actlibrary.tc.faa.gov in Adobe Acrobat portable document format (PDF).

Technical Report Documentation Page

1. Report No.	2. Government Accession No.	3. Recipient's Catalog No.
DOT/FAA/AR-05/21		

4. Title and Subtitle	5. Report Date
HANDLING QUALITIES AND FLIGHT SAFETY IMPLICATIONS OF RUDDER CONTROL STRATEGIES AND SYSTEMS IN TRANSPORT AIRCRAFT	June 2005
	6. Performing Organization Code
7. Author(s)	8. Performing Organization Report No.
Ronald A. Hess	
9. Performing Organization Name and Address	10. Work Unit No. (TRAIS)
Dept. of Mechanical and Aeronautical Engineering University of California Davis, CA 95616	11. Contract or Grant No.
12. Sponsoring Agency Name and Address	13. Type of Report and Period Covered
U.S. Department of Transportation Federal Aviation Administration Office of Aviation Research Washington, DC 20591	Final Report
	14. Sponsoring Agency Code
	ANM-100

15. Supplementary Notes

The FAA William J. Hughes Technical Center Manager was Robert McGuire.

16. Abstract

An analytical and limited experimental study was undertaken to assess the effects of rudder control systems and strategies in transport aircraft. The analytical study encompassed a pilot and vehicle analysis of possible feedback strategies that could be used by a transport aircraft pilot for lateral and directional control. The effect of control sensitivity was accounted for in approximate fashion in the analyses. Pilot-induced oscillation tendencies were examined. The experimental study involves a desktop, human-in-the-loop simulation of the tasks used in the analytical study. A final comparison was undertaken involving pedal force/displacement characteristics for three transport aircraft and a helicopter. A simple index was proposed that can quantify the linearity of the force/displacement characteristics of any force/feel system.

17. Key Words	18. Distribution Statement
Rudder control, Feedback strategies, Transport aircraft, Human-in-the-loop simulation, Pedal force/displacement characteristics	This document is available to the public through the National Technical Information Service (NTIS) Springfield, Virginia 22161.

19. Security Classif. (of this report)	20. Security Classif. (of this page)	21. No. of Pages	22. Price
Unclassified	Unclassified	57	

Form DOT F1700.7 (8-72) Reproduction of completed page authorized

ACKNOWLEDGEMENT

The research reported herein was supported by a grant from the Federal Aviation Administration through the Airport and Aircraft Safety R&D Division at the William J. Hughes Technical Center, Atlantic City International Airport, NJ. The grant technical manager was Robert McGuire.

TABLE OF CONTENTS

		Page
EXECUTIVE SUMMARY		xi
1.	ANALYTICAL STUDY	1
1.1	Introduction	1
1.2	Rudder Feedback Strategies for Manual Control	1
1.2.1	Yaw Rate to Rudder	1
1.2.2	Sideslip to Rudder	2
1.2.3	Roll Attitude to Rudder	2
1.2.4	Roll Attitude to Aileron	2
1.2.5	Roll Attitude to Rudder and Aileron (Coordinated Control)	2
1.2.6	Frequency-Domain Comparisons	3
1.2.7	Handling Qualities Implications of Coordinated Control	5
1.3	Pilot Models for Computer Simulation	7
1.3.1	Introduction	7
1.3.2	Pilot Model for Single-Axis Tracking	8
1.3.3	Coordinated Aileron and Rudder Inputs	11
1.3.4	Piloting Tasks for Computer Simulation	13
1.4	Suggestions for Flight Simulator Investigations	22
1.5	Summary of Section 1	22
2.	DESKTOP SIMULATION	23
2.1	Introduction	23
2.2	Visual Scene Representation	23
2.3	Inceptor	24
2.4	Aerodynamic Model	25
2.5	Control Law Implementation	26
2.6	Test Subject	27
2.7	Simulation Results	27
2.7.1	Task 1: Large Roll Attitude Change	27
2.7.2	Task 2: Wings-Level Sideslip Captures	32
2.8	Summary of Section 2	35
3.	PEDAL FORCE/FEEL SYSTEM COMPARISON	35
3.1	Introduction	35

3.2 The Helicopter Comparison 37
3.3 Comparing Pedal Force/Feel Characteristics 37
3.4 A Computer Simulation 38
3.5 Summary of Section 3 43

4. SUMMARY OF RESULTS 44

5. CONCLUSIONS 44

6. REFERENCES 45

LIST OF FIGURES

Figure Page

1 Bode Diagrams of $\frac{r}{\delta_r}(s)$ Without and With Yaw Damper 3

2 Bode Diagrams of $\frac{\beta}{\delta_r}(s)$ Without and With Yaw Damper 4

3 Bode Diagrams of $\frac{\phi}{\delta_r}(s)$ With and Without Yaw Damper 4

4 Bode Diagrams of $\left.\frac{\phi}{\delta_a}\right|_{\delta_r = K_r \cdot \delta_a}(s)$ With Yaw Damper for K_r = 0, 0.25, 0.5, and 0.75, Including Aileron and Rudder Actuator Models 5

5 Bandwidth and Phase Delay Definitions 6

6 Bode Diagram of $\left.\frac{a_{y_{ps}}}{\delta_a}(s)\right|_{\delta_r = 0.75\delta_a}$ 7

7 The Structural Model of the Human Pilot 8

8 Structural Pilot Model for Roll Attitude to Aileron Control 10

9 Pilot/Vehicle System for Coordinated Use of Aileron and Rudder 12

10 Bode Diagram of Open Loop Pilot/Vehicle Transfer Function With K_r = 0 13

11	Computer Simulation of Pilot/Vehicle System With Aileron Input Alone (K_r = 0) and With Coordinated Aileron and Rudder Inputs (K_r = 0.25, 0.50, and 0.75)	14
12	Aileron and Rudder Inputs for Tracking Figure 11, K_r = 0	14
13	Aileron and Rudder Rates for Tracking Figure 11, K_r = 0	15
14	Aileron and Rudder Inputs for Tracking Figure 11, K_r = 0.5	15
15	Aileron and Rudder Rates for Tracking Figure 11, K_r = 0.5	16
16	Lateral Acceleration in the Cockpit for Tracking Figure 12, K_r = 0 and K_r = 0.5	16
17	Lateral Acceleration in the Cockpit for Tracking Figure 12, K_r = 0, K_r = 0.5, and K_r = 0.35 With High Rudder Sensitivity	17
18	Rudder and Aileron Inputs in Simulated PIO With Pilot Model Adopting Regressive Behavior (PIO frequency 3 rad/sec)	18
19	Pilot/Vehicle System for Roll Attitude to Aileron and Sideslip to Rudder	19
20	Bode Diagrams of Open Loop Pilot/Vehicle Transfer Functions for Roll and Sideslip Loops	19
21	Computer Simulation of Pilot/Vehicle System to Alternating Sideslip Commands	20
22	Aileron and Rudder Inputs for Tracking Figure 21	20
23	Aileron and Rudder Rates for Tracking Figure 21	21
24	Lateral Acceleration in the Cockpit for Tracking Figure 21	21
25	Rudder and Aileron Inputs in Simulated PIO With Pilot Model Adopting Regressive Behavior (PIO frequency 2.9 rad/sec)	22
26	Visual Scene Representation in Desktop Simulation	23
27	Visual Scene Representation With Plastic Overlay	24
28	Physical Simulation Setup	25
29	Simulation Details in HPESIM	26
30	Control Law Implementation Scheme in HPESIM (Longitudinal Axis Shown)	26
31	Large Roll Attitude Change Task, Wheel Only Subject Inputs	27
32	Aileron and Rudder Inputs for Task of Figure 31	28

33	Aileron and Rudder Rates for Task of Figure 31	28
34	Large Roll Attitude Change Task, Wheel and Pedal Inputs	29
35	Aileron and Rudder Inputs for Task of Figure 34	29
36	Aileron and Rudder Rates for Task of Figure 34	29
37	Comparison of Lateral Acceleration at Pilot's Station (a_{ps}) for Tasks of Figures 31 and 34	30
38	Large Roll Attitude Change Task, Wheel and Pedal Inputs, Performed With Low-Gain Tracking Behavior	30
39	Aileron and Rudder Inputs for Task of Figure 38	31
40	Aileron and Rudder Rates for Task of Figure 38	31
41	Large Roll Attitude Change Task, Wheel and Pedal Inputs, Performed With Transient Rudder Inputs	31
42	Aileron and Rudder Inputs for Task of Figure 41	32
43	Aileron and Rudder Rates for Task of Figure 38	32
44	Sideslip and Roll Attitude in Sideslip Capture Task	33
45	Aileron and Rudder Inputs for Task of Figure 44	33
46	Aileron and Rudder Rates for Task of Figure 44	33
47	Modified Sideslip Capture Task	34
48	Aileron and Rudder Inputs for Task of Figure 47	34
49	Aileron and Rudder Rates for Task of Figure 47	34
50	Pedal Force/Feel System Comparison of the A300-600 at 240 kts and the UH-60A Blackhawk Helicopter	36
51	Pedal Force/Feel System Comparison of the B-767 and the UH-60A Blackhawk Helicopter	36
52	Pedal Force/Feel System Comparison of the Airbus A300-B2-B4 and the UH-60A Blackhawk Helicopter	37
53	A Simplified Computer Model of the Pilot/Vehicle System	38

54 Representation of the Pedal Force/Feel Systems A and B in the Computer Simulation of Figure 53 39

55 Responses of the Computer Simulation System of Figure 53 for Different Pilot Gains for the System A Pedal Force/Feel System 40

56 Responses of the Computer Simulation System of Figure 53, for Different Pilot Gains for System B Pedal Force/Feel System 40

57 Pedal Force vs Pedal Displacement for Systems A and B in Figure 53 for $K_p = 4$ 41

58 Defining a Linearity Index 42

59 Alternate Definition of Linearity Index 43

LIST OF TABLES

Table Page

1 Bandwidth and Phase Delay for Systems of Figure 4 6
2 Force/Feel System Summary 38

LIST OF ACRONYMS

LI	Linearity index
PIO	Pilot-induced oscillations
PS	Pilot’s station

EXECUTIVE SUMMARY

This report contains five sections. Section 1 contains an analytical investigation of various rudder control strategies that could be employed by the pilot of a transport aircraft. A detailed mathematical model of the human pilot is used in a computer simulation to examine the closed-loop nature of these strategies. It is shown that the coordinated or combined use of aileron and rudder inputs for roll-attitude tracking can exhibit poor performance and stability compared to a strategy using aileron inputs alone. It is also suggested that rudder force/feel systems with large sensitivities (low force gradients) can precipitate lateral/directional pilot-induced oscillations with coordinated rudder and aileron inputs due to large lateral accelerations being created at the pilot's station. Similar large accelerations at the pilot's station can be created in a sideslip capture task when large control sensitivities exist in the rudder control system. These accelerations can also serve as a trigger for pilot-induced oscillations.

Section 2 involves a human-in-the-loop desktop simulation of the rudder control strategies examined in section 1. In particular, the handling qualities and potential flight safety problems of high-gain, closed-loop tracking using coordinated or combined aileron and rudder inputs predicted in section 1 appear in the simulations of section 2.

Section 3 discusses a comparison of the rudder force/feel characteristics of three transport aircraft and a military helicopter. Significant differences in the force/feel characteristics of one transport compared to the remaining two and the helicopter are noted. A linearity index is defined to quantify the linear force/displacement characteristics of any force/feel system. A simple computer simulation of a closed-loop piloting task involving two of the force/feel systems differing most in linearity indicates that the nonlinear force/feel design leads to unpredictable vehicle responses and poor performance.

Section 4 summarizes the major results of the study.

Section 5 presents the major conclusions.

Section 6 lists the references cited in this report.

1. ANALYTICAL STUDY.

1.1 INTRODUCTION.

The Federal Aviation Administration has undertaken a four-phase research project to study airplane rudder control systems. The four phases include Literature and Database Review, Pilot Survey, Desk Top Simulation, and Real-Time Pilot Simulation. This report represents part of the third phase Desk Top Simulation.

Recent incidents, like the crash of American Airlines Flight 587 in November 2001, have brought transport pilots' use of rudder control under increased scrutiny [1-3]. This is especially true in large upsets caused by wake vortex encounters [4]. Rudder designs are typically driven by the following general requirements: (1) maintaining zero sideslip in turning flight, i.e., overcoming adverse yaw; (2) maintaining or minimizing sideslip in asymmetric power conditions, e.g., power loss in multiengine aircraft; (3) maintaining constant sideslip in crosswind landings; and (4) spin recovery. None of these requirements are directed toward using the rudder in closed-loop tracking control, an activity that will be of central importance in the research to be described.

1.2 RUDDER FEEDBACK STRATEGIES FOR MANUAL CONTROL.

Reference 5 presents a thorough treatment of various feedback strategies (or surveys) using the rudder as part of automatic feedback system, i.e., stability augmentation systems. Three systems were of particular interest to this study: feedback of yaw rate to rudder, $r \rightarrow \delta_r$; sideslip to rudder, $\beta \rightarrow \delta_r$; and roll attitude to rudder, $\phi \rightarrow \delta_r$, particularly in combination with aileron to rudder, $\phi \rightarrow \delta_r$, δ_a. Reference 6, published nearly 40 years ago, provides an analytical and experimental study of lateral directional manual control. This involved feedback of roll attitude to aileron, $\phi \rightarrow \delta_a$, and yaw rate to rudder, $r \rightarrow \delta_r$.

1.2.1 Yaw Rate to Rudder.

The yaw-rate-to-rudder deflection transfer function for a typical transport aircraft can be given in symbolic fashion as [5]

$$\frac{r}{\delta_r}(s) = \frac{A_r[s^2 + 2\varsigma_r\omega_r s + \omega_r^2]}{(s + 1/T_s)[s^2 + 2\varsigma_d\omega_d s + \omega_d^2]} = \frac{A_r[\varsigma_r, \omega_r]}{(1/T_s)[\varsigma_d, \omega_d]} \tag{1}$$

where the far right-hand side of the equation is expressed in shorthand notation. If a yaw damper is included in the system, mechanized with feedback of first-order, washed-out yaw rate, the general form of equation 1 is modified. A real zero is added (with a time constant equal to the washout pole) as well as a real pole with a slightly smaller time constant than the washout pole. In this case, δ_r would represent the output of the pedal force/feel system in the cockpit, with the yaw damper loop closed. No actuator dynamics are included at this juncture.

1.2.2 Sideslip to Rudder.

The sideslip-to-rudder deflection transfer function for a typical transport aircraft can also be given in symbolic fashion as

$$\frac{\beta}{\delta_r}(s) = \frac{A_\beta (1/T_{\beta_1})(1/T_{\beta_2})(1/T_{\beta_3})}{(1/T_s)(1/T_r)[\varsigma_r, \omega_r]} \tag{2}$$

Taken alone, feedback of sideslip to rudder can destabilize the spiral mode emanating from the root at s = -1/T_s [5]. If a yaw damper with feedback of first-order, washed-out yaw-rate is included, a modification similar to that for the yaw rate-to-rudder transfer function occurs.

1.2.3 Roll Attitude to Rudder.

The roll attitude-to-rudder deflection transfer function for a typical transport aircraft can be given in symbolic fashion as

$$\frac{\phi}{\delta_r}(s) = \frac{A_\phi (1/T\phi_1)(1/T\phi_2)}{(1/T_s)(1/T_r)[\varsigma_r, \omega_r]} \tag{3}$$

It should be noted that the zero $s = -1/T_{\phi_2}$ will typically be nonminimum phase and can possess a relatively small time constant, i.e., on the same order as the roll subsidence mode. The addition of a yaw damper will have a similar effect as in the previous two cases. The appearance of the nonminimum phase zero and resulting reverse action in control response is attributable to the fact that the rudder induces yawing as well as rolling motion. Initially, a rudder deflection will induce a rolling motion opposite to the intended input. Quickly, however, a sideslip develops that induces the desired roll response.

1.2.4 Roll Attitude to Aileron.

The roll attitude-to-aileron deflection transfer function for a typical transport aircraft can be given by

$$\frac{\phi}{\delta_a}(s) = \frac{A_{\phi_1}[\varsigma_\phi, \omega_\phi]}{(1/T_s)(1/T_r)(\varsigma_d, \omega_d)} \tag{4}$$

The addition of a yaw damper will affect the transfer function in a manner similar to the previous cases.

1.2.5 Roll Attitude to Rudder and Aileron (Coordinated Control).

Here, one considers the possibility that the pilot may employ both aileron and rudder to control roll attitude. This might occur in a large roll upset where aileron control alone may appear to provide insufficient roll control power. In this case, one can consider

$$\phi(s) = \frac{\phi}{\delta_a}(s)\cdot\delta_a(s) + \frac{\phi}{\delta_r}(s)\cdot\delta_r(s)\Big|_{\delta_r = K_r\cdot\delta_a}$$

$$\phi(s) = \frac{\phi}{\delta_a}(s)\cdot\delta_a(s) + \frac{\phi}{\delta_r}\cdot K_r\cdot\delta_a(s) \tag{5}$$

$$\frac{\phi}{\delta_a}(s) = \frac{\phi}{\delta_a}(s) + \frac{\phi}{\delta_r}\cdot K_r$$

In equation 5, it is assumed that rudder inputs proportional to aileron inputs are commanded with the relation between the two inputs given by $\delta_r = K_r \cdot \delta_a$.

1.2.6 Frequency-Domain Comparisons.

Figures 1 through 3 show the Bode diagrams of the transfer functions in equations 1 through 3 for a generic transport aircraft. This aircraft is the DC-8 vehicle with stability derivatives defined for flight condition 8002 in reference 5, corresponding to an airspeed of 468.2 ft/sec and an altitude of 15,000 ft. Also shown are the diagrams that result when washed-out yaw rate is fed back to the rudder. The yaw damper transfer function is given by

$$\frac{\delta_r}{r}(s) = \frac{1.14(0)}{(0.5)}\ rad/rad \tag{6}$$

with the gain being chosen as one which increases the damping of the dutch roll mode from 0.11 to 0.4. The Bode diagrams in figures 1 through 3 clearly show the increase in dutch roll mode damping provided by the yaw damper. The magnitude and phase characteristics of figure 3 clearly show the effects of the nonminimum phase zero, here at s = -2.56.

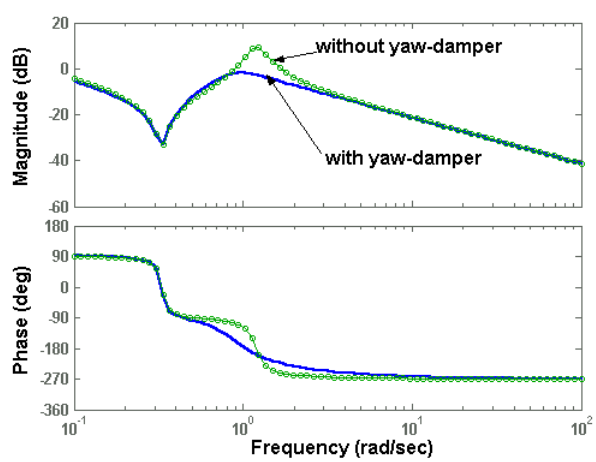

FIGURE 1. BODE DIAGRAMS OF $\frac{r}{\delta_r}(s)$ WITHOUT AND WITH YAW DAMPER

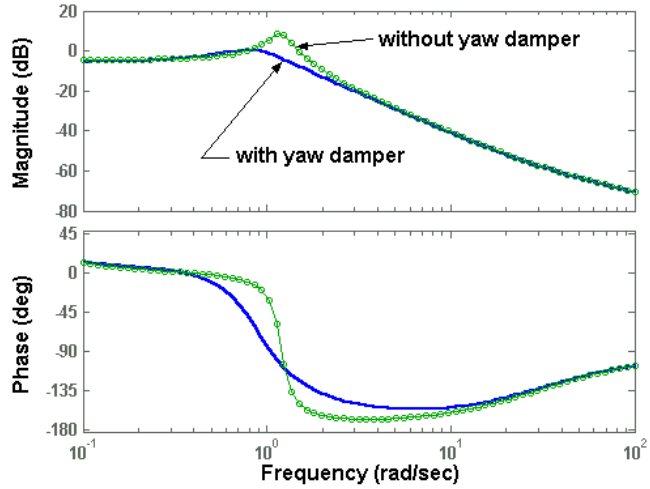

FIGURE 2. BODE DIAGRAMS OF $\frac{\beta}{\delta_r}(s)$ WITH AND WITHOUT YAW DAMPER

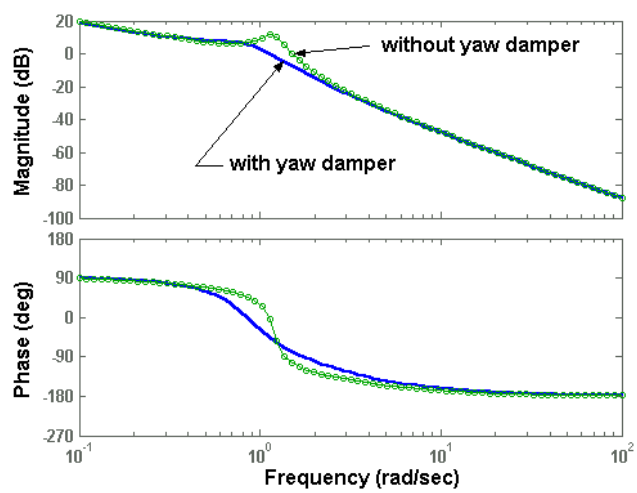

FIGURE 3. BODE DIAGRAMS OF $\frac{\phi}{\delta_r}(s)$ WITH AND WITHOUT YAW DAMPER

Figure 4 shows the Bode diagrams for the system of the last of equation 5 for K_r = 0, 0.25, 0.5, and 0.75. The yaw damper of equation 6 is included in each of these systems as are two actuator models for aileron and rudder. These actuator models are given by

$$\frac{\delta_r}{\delta_{r_c}} = \frac{\delta_a}{\delta_{a_c}} = \frac{20^2}{[0.707,20]} \quad rad/rad \tag{7}$$

As will be discussed in section 1.3, the value of K_r = 0.75 will produce the maximum-allowable rudder input when the aileron input is also the maximum allowable.

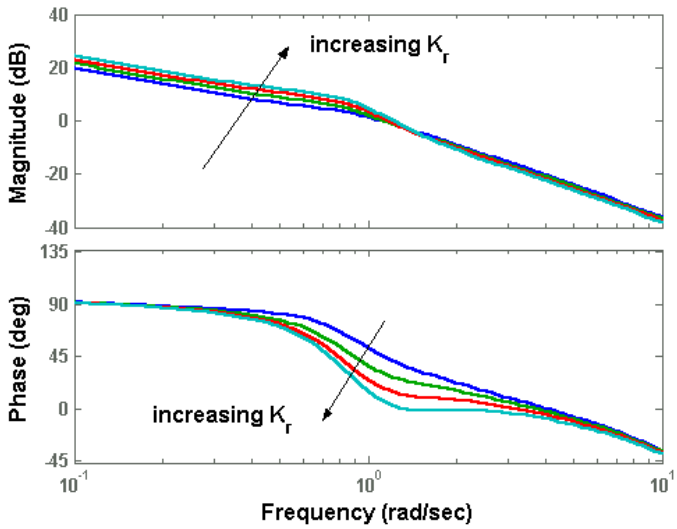

FIGURE 4. BODE DIAGRAMS OF $\left.\frac{\phi}{\delta_a}\right|_{\delta_r = K_r \cdot \delta_a}(s)$ WITH YAW DAMPER FOR K_r = 0, 0.25, 0.5, AND 0.75, INCLUDING AILERON AND RUDDER ACTUATOR MODELS

For frequencies less than 1 rad/sec, the Bode diagrams in figure 4 show that an increase in roll control power can be obtained with the combined use of rudder and aileron. In the case of K_r = 0.75, the increase is approximately a factor of 1.7. In addition, the magnitude and phase curves in this low frequency range show the K/s—like characteristics long associated with desirable handling qualities (180° should be subtracted from the phase curves to account for the sign definitions of positive rudder and aileron). The same cannot be said for higher frequencies however. The magnitude characteristics for all K_r values indicate a first-order lag appearing around 1 rad/sec. As K_r increases, however, phase lags beyond the 90° associated with a first-order lag can clearly be seen.

1.2.7 Handling Qualities Implications of Coordinated Control.

So-called coordinated control of aileron and rudder may constitute the most challenging pilot feedback strategies in terms of vehicle handling qualities. Bandwidth and phase delay have been used extensively for handling qualities investigations, e.g., reference 7. While the particular values of these parameters would be dependent upon the particular aircraft model selected here, the relative variations in these parameters as a function of K_r can shed light upon the handling qualities variations that may occur with coordinated use of rudder and aileron. Figure 5 shows the definitions of bandwidth and phase delay [7]. The Bode diagrams in figure 4 indicate that the response is a rate-type system. Using the definitions given in figure 5, the bandwidth and phase delay results for the four transfer functions in figure 4 are given in table 1.

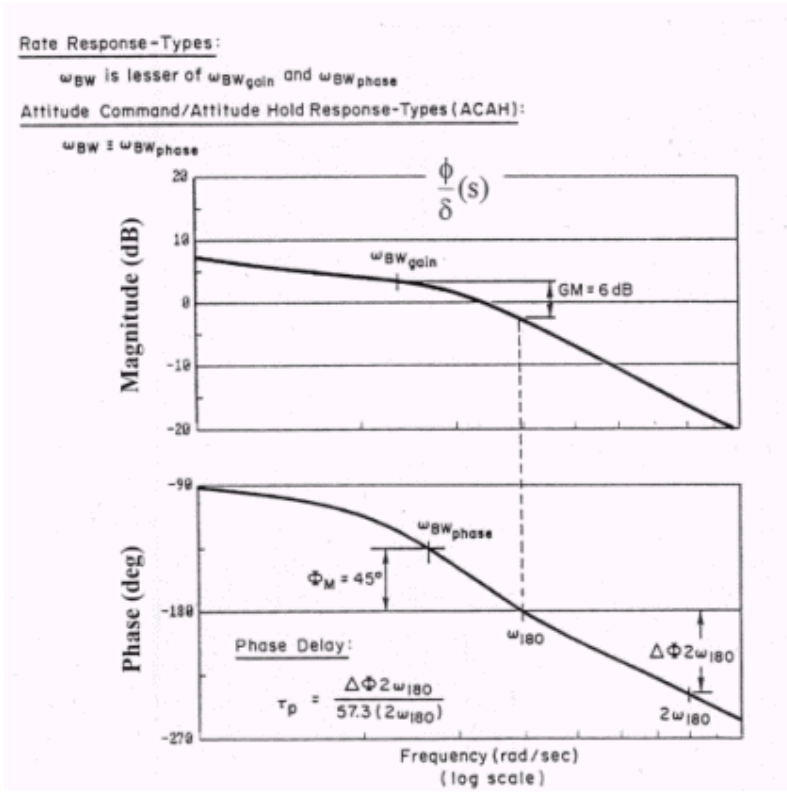

FIGURE 5. BANDWIDTH AND PHASE DELAY DEFINITIONS

TABLE 1. BANDWIDTH AND PHASE DELAY FOR SYSTEMS OF FIGURE 4

K_r	Bandwidth (rad/sec)	Phase Delay (sec)
0	1.14†	0.06
0.25	0.90	0.055
0.5	0.792	0.054
0.75	0.738	0.013

† All bandwidths obtained from $\omega_{BW_{phase}}$

The most significant feature of the results of table 1 is the significant decrease in bandwidth as K_r increases. It must be emphasized that the results of table 1 correspond to a hard-wired aileron and rudder linkage. In reality, this linkage is created by the pilot. Of particular interest to this study is the susceptibility of an aircraft to pilot-induced oscillations (PIO). Unfortunately, at present, no PIO boundaries have been established for bandwidth (as opposed to those for phase delay). As pointed out in reference 8, this is due to a lack of supporting data, not to any assumption as to the possible impact of roll bandwidth on PIO. Thus, a direct comparison with existing bandwidth and phase delay boundaries that delineate handling qualities levels, (e.g., reference 7) must be approached with caution.

The small phase delays in table 1 are attributable to the shape of the phase curves in the frequency range beyond the point where the phase lags equal -180°. That is, the phase curves do not resume a steep roll off until frequencies associated with the bandwidths of the actuators are reached.

If manual control of roll attitude through coordinated use of rudder and aileron is attempted, the resulting lateral accelerations at the pilot's station (PS) are also pertinent to a discussion of handling qualities. The lateral acceleration to aileron transfer function then can be approximated as [5]

$$\frac{a_{y_{ps}}}{\delta_a}(s) \approx Y_v \frac{v}{\delta_a}(s)\bigg|_{\delta_r = K_r \delta_a} + Y_{\delta_r} \cdot K_r + x_{ps} \frac{\dot{r}}{\delta_a}(s)\bigg|_{\delta_r = K_r \delta_a} \tag{8}$$

where x_{ps} is the x body-axis coordinate of the pilot's station. Figure 6 shows the Bode diagrams of the transfer function of equation 8 for the example vehicle. Here, the yaw damper and rudder actuator are included and K_r = 0.75.

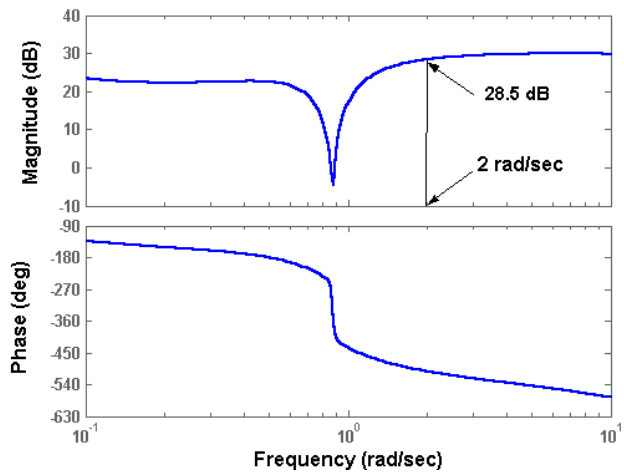

FIGURE 6. BODE DIAGRAM OF $\frac{a_{y_{ps}}}{\delta_a}(s)\bigg|_{\delta_r = 0.75\delta_a}$

Figure 6 indicates that if a sinusoidal aileron input of $\delta_a(t)$ = 20sin(2t) deg with an associated $\delta_r(t)$ = (15) sin(2t) deg is applied, the resulting amplitude of the sinusoidal lateral acceleration at the PS will be approximately 9.2 ft/sec^2 or 0.24 g's.

1.3 PILOT MODELS FOR COMPUTER SIMULATION.

1.3.1 Introduction.

The fundamental manual control theory states that the pilot will provide whatever compensation is necessary to yield an open loop pilot/vehicle transfer function that resembles *K/s* in the region

of the open loop crossover frequency [9]. This representation has been referred to as the Crossover Model of the human pilot and can be represented as

$$Y_p Y_c \approx \frac{\omega_c e^{-\tau_e s}}{s} \tag{9}$$

where Y_p represents the pilot transfer function and Y_c represents the vehicle for the control axis in question. Also in equation 9, ω_c represents the crossover frequency and τ_e represents an effective delay. The latter encompasses true transport delays in the human central nervous system, delays that approximate the higher-frequency human neuromotor dynamics, and higher-frequency vehicle dynamics that may be omitted from Y_c. In what follows, two different tasks and feedback strategies will be examined. First, coordinated use of aileron and rudder will be examined (including no rudder usage). Second, the piloted control of roll attitude with aileron and sideslip with rudder will also be examined. The first of these tasks might model the pilot using aileron and rudder to provide rapid roll attitude recovery from an upset. The second task could represent a situation in which the pilot is attempting to maintain a given heading with wings level, while a transient crosswind creates an effective sideslip angle.

1.3.2 Pilot Model for Single-Axis Tracking.

To create a realistic computer simulation of the pilot/vehicle system, a more complete pilot model than that implied by equation 9 is obviously needed. This will be accomplished by using the structural model of the human pilot, e.g., reference 10. Figure 7 shows the structural pilot/vehicle model appropriate for single-axis tracking of roll attitude, here with aileron inputs, alone. Thus, in figure 7, $C \equiv \phi_c$, $M \equiv \phi$, and $\delta \equiv \delta_w$, the displacement of the wheel (output of the wheel force/feel system). Referring to figure 7, the following pilot model elements can be given.

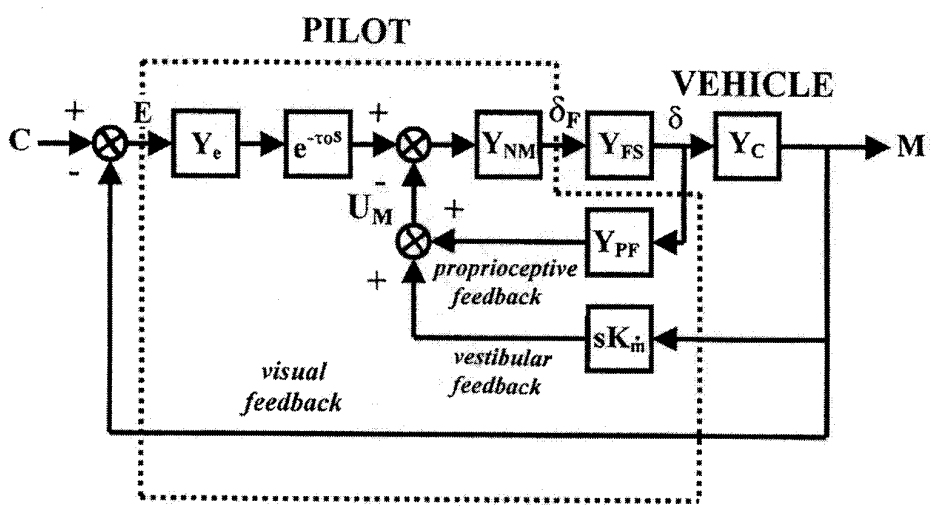

FIGURE 7. THE STRUCTURAL MODEL OF THE HUMAN PILOT

- Visual Gain $Y_e = K_e$. The value of this gain is application-dependent and is selected to yield a desired open loop crossover frequency [9].

- Time Delay τ_0. This delay is selected as 0.2 sec and models human delay sources exclusive of those associated with neuromuscular system operation.

- Neuromuscular System Dynamics. These dynamics are modeled as

$$Y_{NM} = \frac{10^2}{s^2 + 2(0.707)10s + 10^2} \tag{10}$$

  and represent the actuation dynamics of the particular limb effecting control, e.g., arm in wheel motion and leg in pedal motion.

- Proprioceptive System Dynamics. In this particular task, these dynamics are modeled as

$$Y_{PF} = \frac{K_{PF}}{(s + \frac{1}{T_{PF}})} \tag{11}$$

  This form is appropriate for the roll attitude dynamics of figure 4, since the pole in proprioceptive feedback dynamics will create a zero in the pilot transfer function located as $s = -1/T_{PF}$.

- Vestibular System Dynamics. For simplicity, no continuous vestibular feedback will be considered in the model, i.e., $K_{\dot{m}} = 0$.

- Force/Feel System Dynamics. The dynamics of the force/feel system(s) will be of the form

$$Y_{FS}(s) = \frac{K_{FS} \cdot \omega_{FS}^2}{s^2 + 2\varsigma_{FS}\omega_{FS}s + \omega_{FS}^2} \quad \textit{displacement/lbf} \tag{12}$$

- Modeling Effects of Control Sensitivity. Control sensitivity, or its reciprocal force gradient, is one of the more important force/feel system parameters affecting handling qualities and particularly PIO susceptibility [11]. Unfortunately, the manner in which the gain K_{PF} is chosen in the structural model removes all control sensitivity effects [10]. However, one important issue can be addressed, which is the ratio between maximum to breakout forces in the force/feel system.

  Figure 8 shows the structural model for a particular application (roll attitude to aileron feedback).

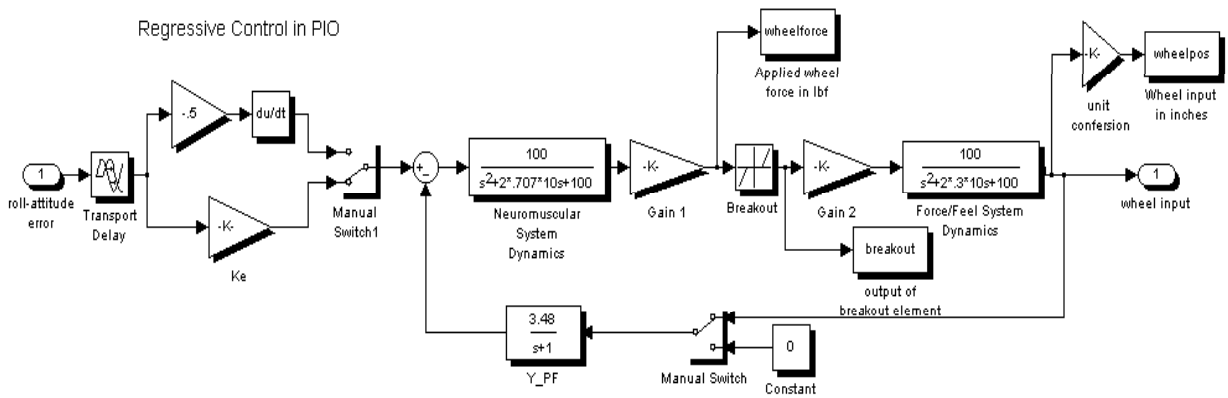

FIGURE 8. STRUCTURAL PILOT MODEL FOR ROLL ATTITUDE TO AILERON CONTROL

In figure 8, an approximation to the control force inputs is obtained by normalizing the signal that represents the model of the neuromuscular dynamics of the particular limb driving the cockpit controller (e.g., the arm moving the wheel). The normalization is defined by the gain value immediately following the neuromuscular system dynamics block in figure 8 (Gain 1 in figure 8). In what follows, inceptor refers to the cockpit controller, e.g., wheel, pedal, etc., and effector refers to the control surface, e.g., aileron, rudder, etc. The gain identified as Gain 1 is defined as

$$K_{force} = \frac{Inceptor\ Force\ Corresponding\ to\ Maximum\ Effector\ Deflection}{Max\ Effector\ Deflection} \tag{13}$$

A nonlinear threshold element follows Gain 1 and represents the breakout characteristics of the inceptor. Because of the preceding gain element, the breakout limits are expressed directly in terms of breakout force. Following the threshold element is another gain (Gain 2) defined simply as the reciprocal of the gain in equation 13. Thus, determination of the force applied by the pilot model is confined to three elements: Gain 1, breakout, and Gain 2. The inceptor displacement is calculated from the output of the force/feel system dynamics by multiplying by a gain (unit conversion in figure 8) defined as

$$K_{displacement} = \frac{Maximum\ Inceptor\ Displacement}{Maximum\ Effector\ Deflection} \tag{14}$$

The threshold element has the effect of a gain reduction in the forward path of the loop closed around the pilot's neuromuscular and force/feel system. By considering the Gaussian input describing function for the threshold nonlinearity that represents the nonlinear force/feel characteristics in the computer simulation [12], this reduced gain can be approximated as[1]

[1] It is assumed in equation 15 that $\sqrt{2\sigma}$ for the Gaussian input to the nonlinearity is equal to $Force|_{max}$.

$$K_{threshold} \approx 1 - \frac{Force|_{breakout}}{Force|_{\max}} = \frac{Force|_{\max} - Force|_{breakout}}{Force|_{\max}} \tag{15}$$

Immediately before the nonlinearity in the Structural Model of the pilot, the reciprocal of the reduced gain is inserted to model the pilot's attempt to compensate for the gain reduction due to the nonlinearity. This latter gain value can be approximated by a multiplicative factor on K_e, defined as follows:

$$K_{factor} = \frac{Force|_{\max}}{Force|_{\max} - Force|_{breakout}} \tag{16}$$

In equations 15 and 16, $Force|_{\max}$ corresponds to Inceptor Force Corresponding to Maximum Effector Displacement in equation 13. Thus, if in equation 16, $Force|_{\max}$ = 25 lbf and $Force|_{breakout}$ = 5 lbf, K_{factor} = 25/20 = 1.25 and the gain K_e is multiplied by 1.25. Since the pilot/vehicle transfer function in any modeling application will have finite stability margins, K_{factor} can induce closed-loop instability if the $Force|_{breakout}$ is of the same order of magnitude as $Force|_{\max}$. Finally, note that if no breakout force is in evidence, the procedure just described will not accommodate the effects of control sensitivity.

1.3.3 Coordinated Aileron and Rudder Inputs.

Referring to figure 4, one sees that, for this task, the pilot would be required to generate first-order lead with a reciprocal time constant on the order of 1/sec, (the approximate location of the dutch roll poles with the yaw damper in place). Thus, in its simplest form, the pilot equalization would be

$$Y_{p_\phi} \approx K_{p_\phi}(s+1) \tag{17}$$

It should also be noted that the form of equation 17 would be invariant with K_r values, since, with the exception of an increase in gain, the form of the various vehicle transfer functions in figure 4 varies only in phase lag. This fact does not bode well for closed-loop system stability at larger values of K_r.

For coordinated use of aileron and rudder, a more complex model than figure 7, must be employed. The hypothesized model is shown in figure 9. Here, the block labeled Structural Model for ϕ-loop is essentially the model of figure 7. It is hypothesized that the command to the pedals is obtained from the input signal to the neuromuscular system for the pilot's arm. The specific parameters for the various elements in figure 9 can now be given.

- Proprioceptive Dynamics. In equation 11, $1/T_{PF}$ = 1/sec. The parameter K_{PF} is chosen as the value that yields a minimum damping ratio of 0.15 for any poles of the transfer function resulting when only the proprioceptive loop of figure 7 is closed.

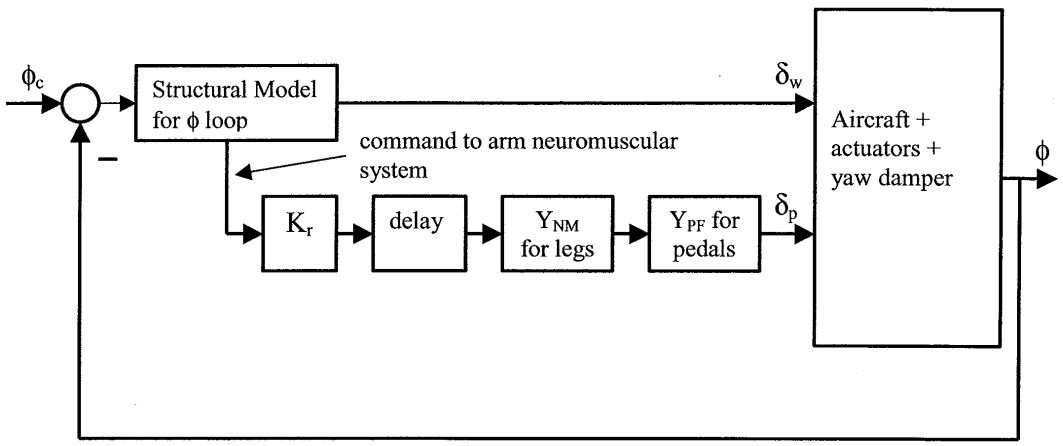

FIGURE 9. PILOT/VEHICLE SYSTEM FOR COORDINATED USE OF AILERON AND RUDDER

- Neuromuscular Dynamics. Y_{NM} will be as given in equation 10 for both arm and legs.

- Force/Feel System Dynamics. Y_{FS} for the wheel and pedals will be given by

$$Y_{FS}\big|_{wheel} = \frac{15 \cdot 10^2}{s^2 + 2(0.3)10s + 10^2} \quad \textit{wheel deflection/lbf} \tag{18}$$

$$Y_{FS}\big|_{pedal} = \frac{65 \cdot 20^2}{s^2 + 2(0.3)20s + 20^2} \quad \textit{pedal deflection/lbf} \tag{19}$$

For the wheel, full deflection corresponds to a 80° wheel rotation and a 20° aileron deflection. For the pedal, full deflection corresponds to 1.5-inch pedal deflection and 15° rudder deflection. The ratio of maximum rudder deflection to maximum aileron deflection is 0.75 and gives rise to the $K_r = 0.75$ value employed in section 1.2. The K_{max} for the aileron is 15 lbf and 65 lbf for the pedals. The breakout forces for the wheel and pedal are wheel: 2 lbf; pedal: 13 lbf.

- Delay. The delay in figure 9 is identical to that in the pilot model of figure 7, 0.2 sec.

- Actuator Dynamics and Limits. The dynamics of the actuators for both rudder and aileron have been given in equation 7. The amplitude and rate limits of these actuators are as follows:

aileron: amplitude limit = ±20°
rate limit = ±45°/sec

rudder: amplitude limit = ±15°
rate limit = ±60°/sec

Figure 10 shows the resulting Bode diagram for the open-loop pilot/vehicle transfer function with K_r = 0, and with K_{factor} set to unity. The diagram is very similar in form to measured pilot/vehicle transfer functions, e.g., reference 9.

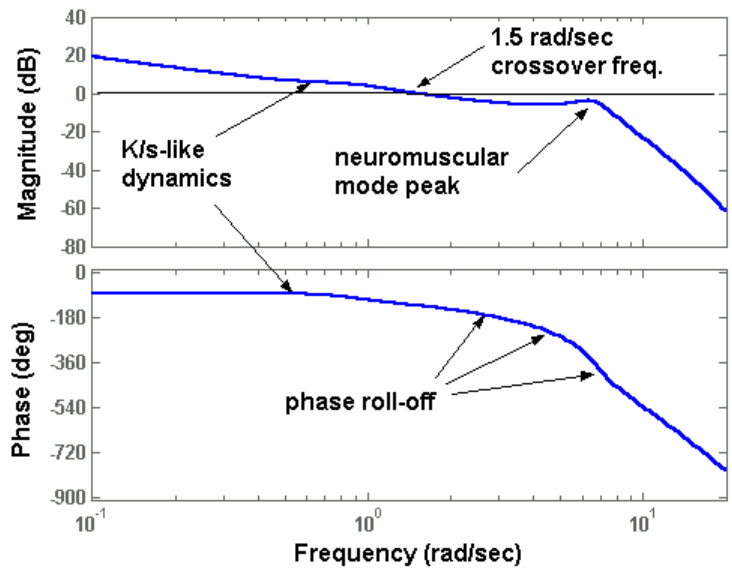

FIGURE 10. BODE DIAGRAM OF OPEN LOOP PILOT/VEHICLE TRANSFER FUNCTION WITH K_r = 0

1.3.4 Piloting Tasks for Computer Simulation.

1.3.4.1 Task 1: Large Roll Attitude Change.

The command roll attitude will be a filtered step command in which the pilot uses the aileron alone with no pedal inputs. Next, the same roll attitude command will be used, but this time, the pilot model will be employing coordinated aileron and pedal inputs. In the second scenario, various K_r values will be chosen, with the largest representing the ratio of maximum displacements of aileron and rudder, i.e., K_r = 0.75.

The crossover frequency for the roll attitude loop with no rudder inputs will be chosen as 1.5 rad/sec. The gain $Y_e = K_e$ selected for the first task will remain unchanged in the second task. The K_{factor} for the aileron loop is from equation 16, K_{factor} = 15/13 = 1.15. For the rudder loop, K_{factor} = 65/52= 1.25. Figure 11 shows the simulation results. When the maximum K_r (0.75) is employed, the closed-loop pilot/vehicle system is unstable, with an oscillatory divergence exhibiting a frequency of 1.5 rad/sec. The results indicate that the dutch roll mode has been excited with the manual loop closures examined here. With K_r = 0 and 0.25, the closed-loop system responds well. The aileron and rudder inputs for each K_r = 0 are shown in figure 12. The residual rudder motion with K_r = 0 is attributable to the action of the yaw damper. Figure 13 shows aileron and rudder rates. Figures 14 and 15 compare aileron and rudder inputs and rates for K_r = 0.5. Figure 16 compares the lateral acceleration in the cockpit for the two K_r values. Note that for K_r = 0.5, the lateral acceleration can reach 0.3 g's. Figures 12 through 15 indicate that amplitude and rate limiting of both aileron and rudder occurs in these tasks.

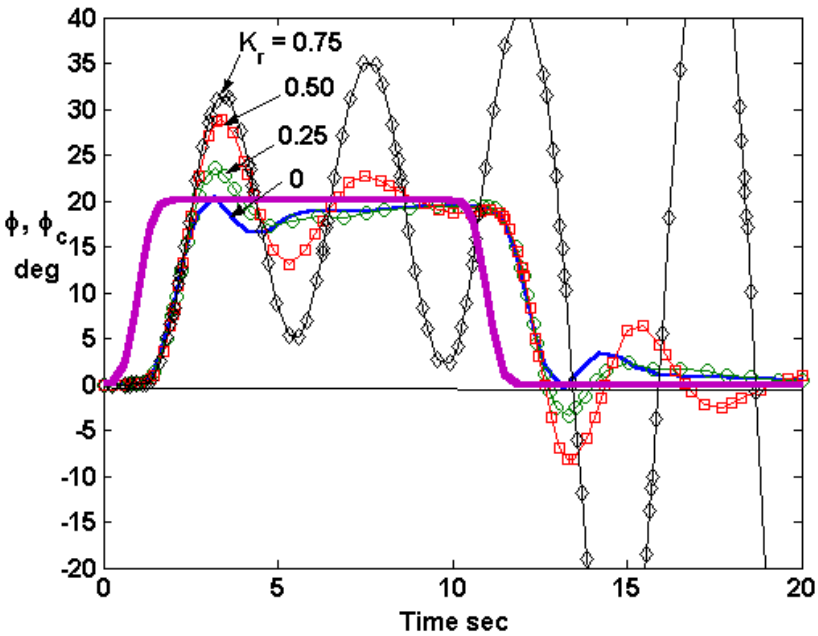

FIGURE 11. COMPUTER SIMULATION OF PILOT/VEHICLE SYSTEM WITH AILERON INPUT ALONE (K_r = 0) AND WITH COORDINATED AILERON AND RUDDER INPUTS (K_r = 0.25, 0.50, AND 0.75)

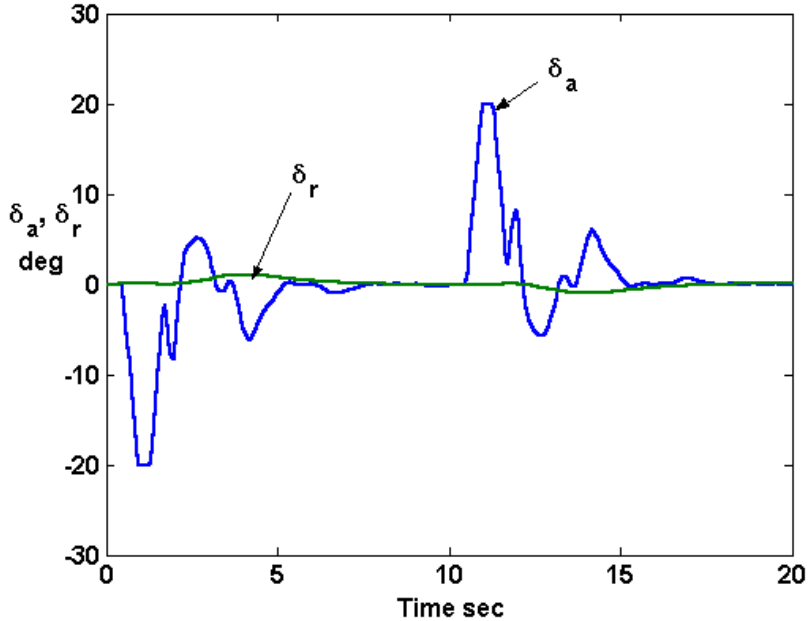

FIGURE 12. AILERON AND RUDDER INPUTS FOR TRACKING FIGURE 11, K_r = 0

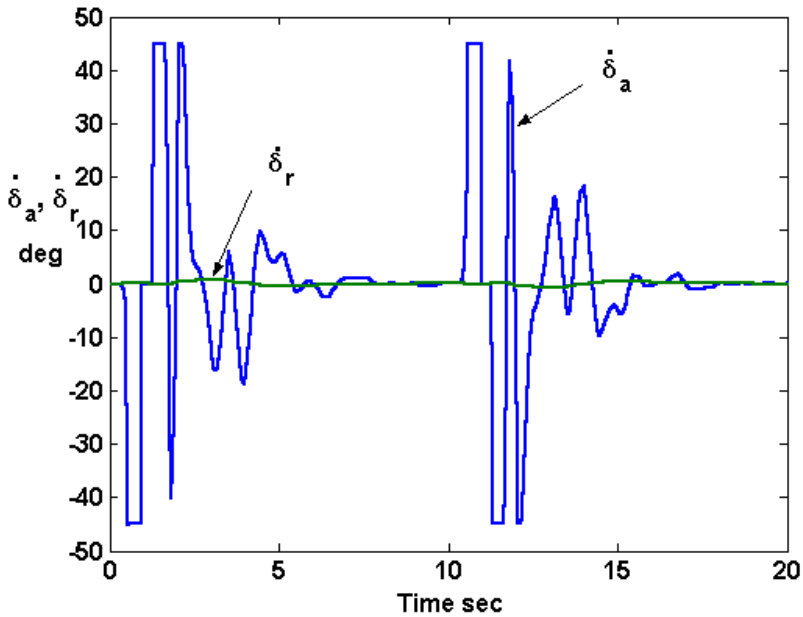

FIGURE 13. AILERON AND RUDDER RATES FOR TRACKING FIGURE 11, $K_r = 0$

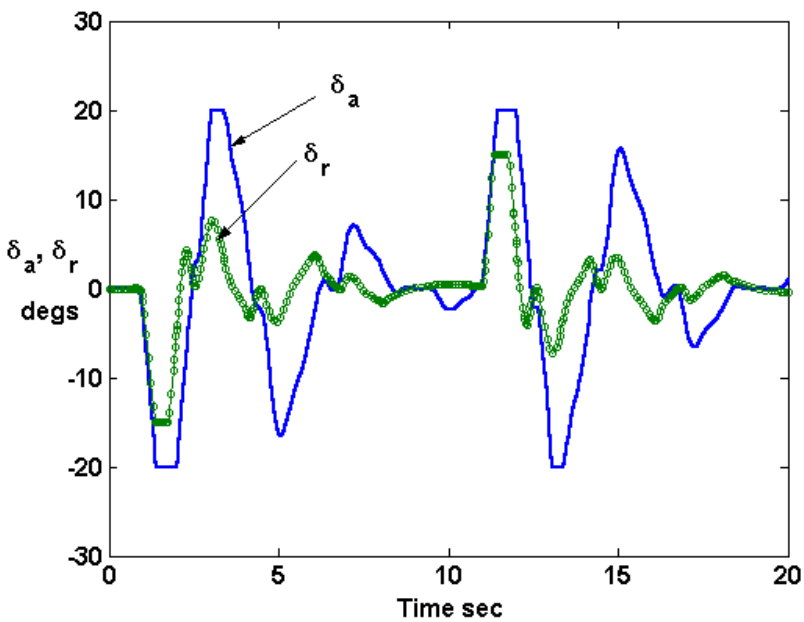

FIGURE 14. AILERON AND RUDDER INPUTS FOR TRACKING FIGURE 11, $K_r = 0.5$

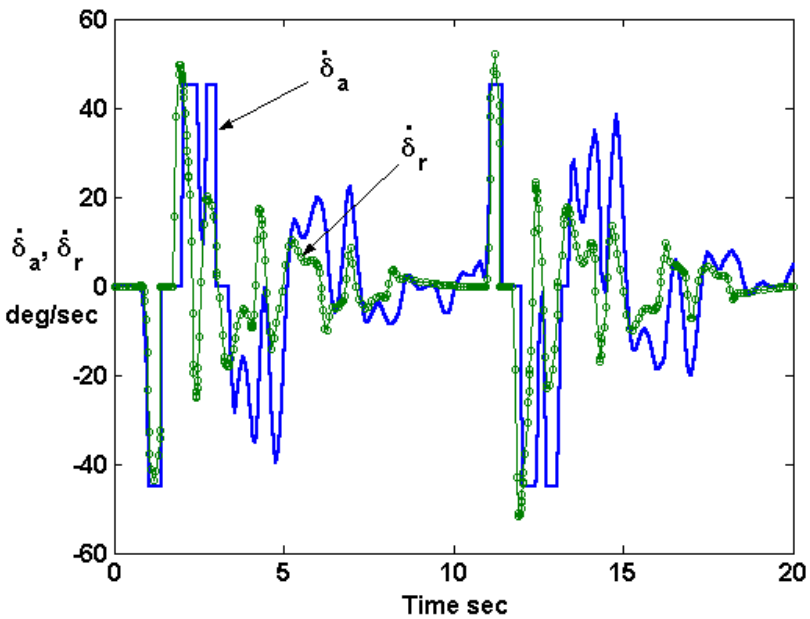

FIGURE 15. AILERON AND RUDDER RATES FOR TRACKING FIGURE 11, K_r = 0.5

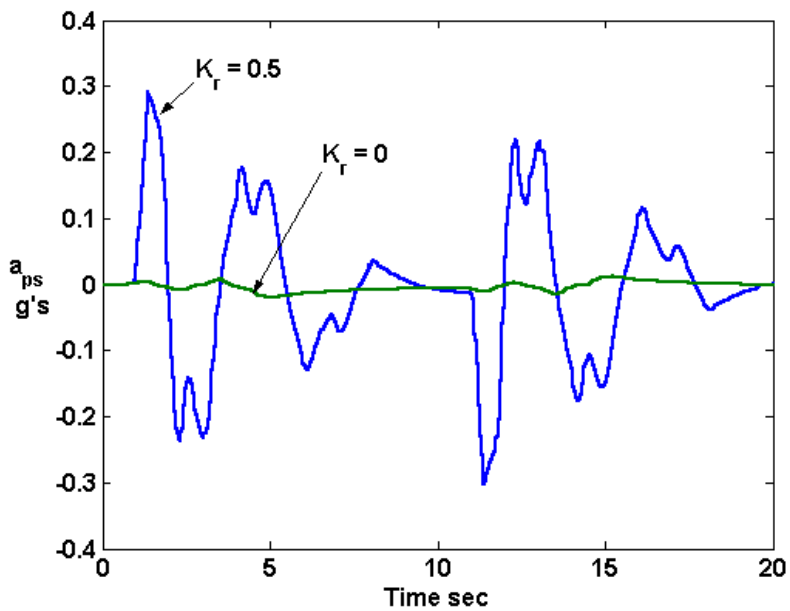

FIGURE 16. LATERAL ACCELERATION IN THE COCKPIT FOR TRACKING FIGURE 12, K_r = 0 AND K_r = 0.5

Figure 17 shows the lateral acceleration in the cockpit that occurs for K_r = 0 and K_r = 0.35 with nominal rudder sensitivity and K_r = 0.35 with high rudder sensitivity, defined here as $K|_{force}$ = 32 lbf and $K|_{breakout}$ = 22 lbf. This yields K_{factor} = 32/10 = 3.2 for the rudder channel. The increased rudder sensitivity has significantly increased the maximum values of a_{ps}.

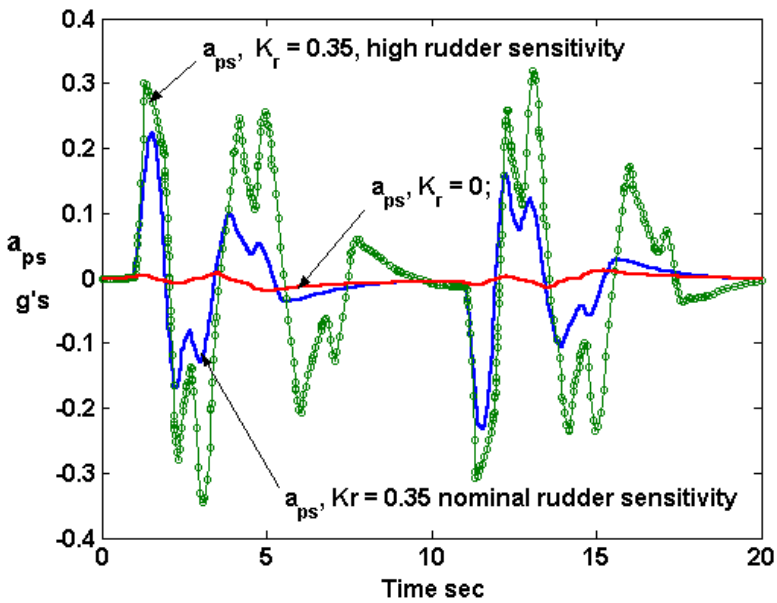

FIGURE 17. LATERAL ACCELERATION IN THE COCKPIT FOR TRACKING FIGURE 12, K_r = 0, K_r = 0.5, AND K_r = 0.35 WITH HIGH RUDDER SENSITIVITY

The issue of whether a pilot would coordinate rudder with aileron, as was done in the computer simulation, is open to question. Obviously, continuous high-gain coordination is detrimental to tracking performance and stability. It is possible, however, that a highly sensitive pedal force/feel system might induce pilot activity of this nature. In addition, the large lateral accelerations that are predicted to develop could precipitate a PIO. This was suggested by the author when investigating the crash of American Airlines Flight 587 [11]. A PIO can be precipitated in the computer simulation by forcing the pilot model to adopt the so-called regressive tracking behavior as discussed in reference 10. In this behavior, the pilot is hypothesized to use roll rate rather than roll attitude as the fundamental visual cue. In addition, proprioceptive cues were assumed to be ignored. Figure 18 shows aileron and rudder inputs demonstrating the oscillatory vehicle responses that develop with this regressive behavior. Here, the minimum pilot gain was selected that yielded the oscillatory behavior. The nature of the aileron and rudder inputs indicate that amplitude and rate saturation of these devices occurred. The frequency of the PIO is approximately 3.0 rad/sec (0.48 Hz).

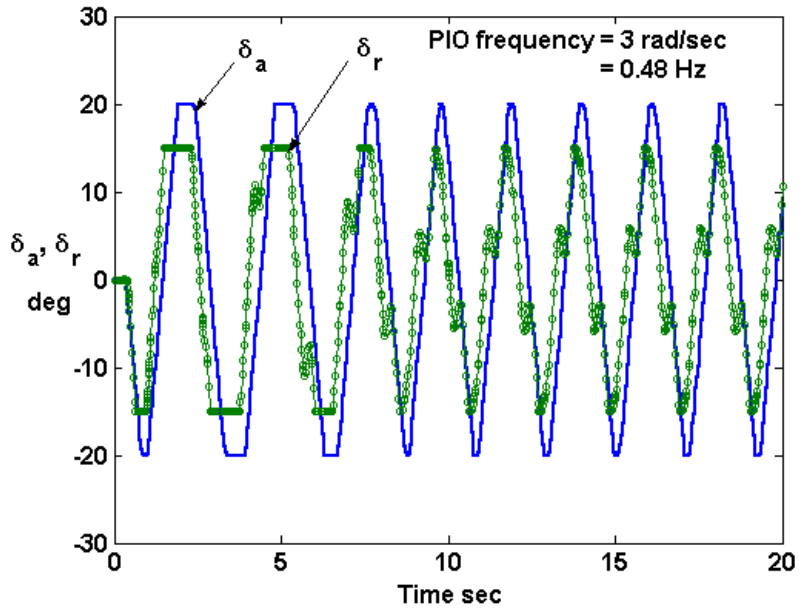

FIGURE 18. RUDDER AND AILERON INPUTS IN SIMULATED PIO WITH PILOT MODEL ADOPTING REGRESSIVE BEHAVIOR (PIO frequency 3 rad/sec)

It should be emphasized that this simulation does not imply that the vehicle chosen for study is PIO prone. Rather that an overly sensitive pedal force/feel system (low force gradient) could precipitate a PIO in a sudden upset by inducing large lateral accelerations at the PS.

1.3.4.2 Task 2: Wings Level Sideslip Captures.

In this task, demanding discrete sideslip captures are required while maintaining wings level.

Referring to figures 2 and 3, one sees that for this task, the pilot would again be required to generate a first-order lead with a reciprocal time constant on the order of 1/sec, for both the aileron and rudder loops. Figure 19 is a block diagram representation of this task. Of course, in flight, sideslip deviations would not be sensed by the pilot as readily as a roll attitude. In a flight simulator, however, sideslip deviations could be presented to the pilot by artificial means. It is the possibility of using such feedback to investigate rudder control in a simulator that motivates this part of the study.

The command roll attitude for this task will be zero, with the sideslip command consisting of a filtered doublet alternating between ±6° in amplitude. One physical interpretation for this input would be the aircraft experiencing a 30-kt wind that alternates between ±30° from the aircraft's initial heading. Here, each alternating pulse lasts approximately 6 sec.

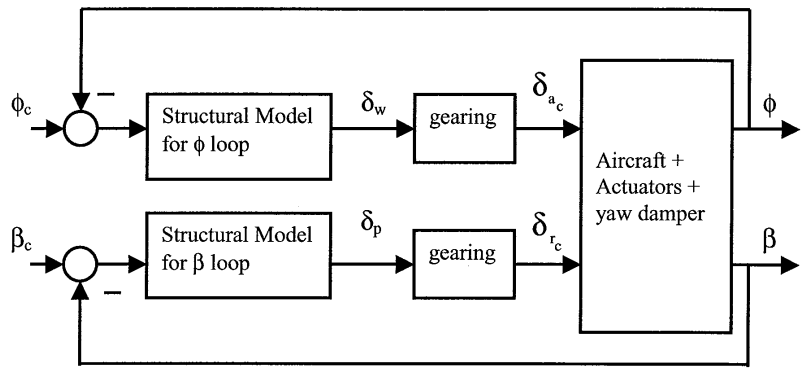

FIGURE 19. PILOT/VEHICLE SYSTEM FOR ROLL ATTITUDE TO AILERON AND SIDESLIP TO RUDDER

Since two loops are being simultaneously closed by the pilot, an iterative procedure is employed to determine the forms of the pilot models for each loop. First, the rudder loop is left open and the appropriate Structural Model pilot dynamics are selected for the aileron loop. As in the study with coordinated aileron and rudder, the general form of Y_{PF} for both loops is as given in equation 11. After selection of the aileron-loop pilot model, this control loop is closed and the appropriate Structural Model pilot dynamics are selected for the sideslip loop. The procedure is repeated until no significant changes in the pilot models occur. Figure 20 shows the Bode diagrams of the open loop pilot/vehicle transfer functions for each loop, with the remaining loop closed.

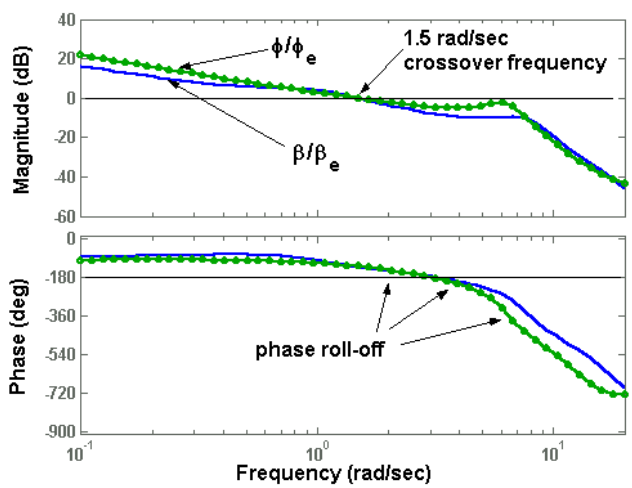

FIGURE 20. BODE DIAGRAMS OF OPEN LOOP PILOT/VEHICLE TRANSFER FUNCTIONS FOR ROLL AND SIDESLIP LOOPS

As was the case in figure 10, K/s-like dynamics are evident, and a common crossover frequency of 1.5 rad/sec is chosen. Once again, this crossover frequency was created with K_{factor} = 1 in each loop.

Figure 21 shows the responses in roll attitude and sideslip. Note the significant roll attitude excursions from the desired wings-level condition. Figures 22 and 23 show the aileron and rudder inputs and rates. Finally, figure 24 shows the resulting lateral acceleration at the PS.

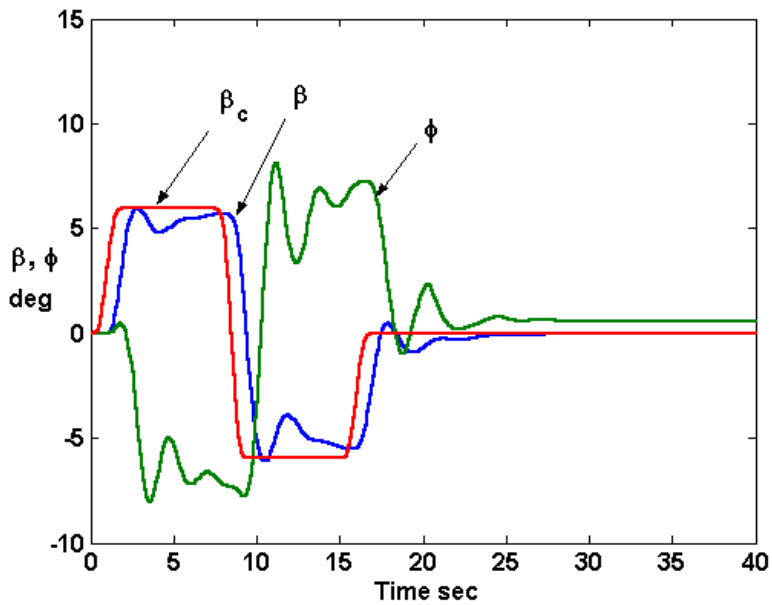

FIGURE 21. COMPUTER SIMULATION OF PILOT/VEHICLE SYSTEM TO ALTERNATING SIDESLIP COMMANDS

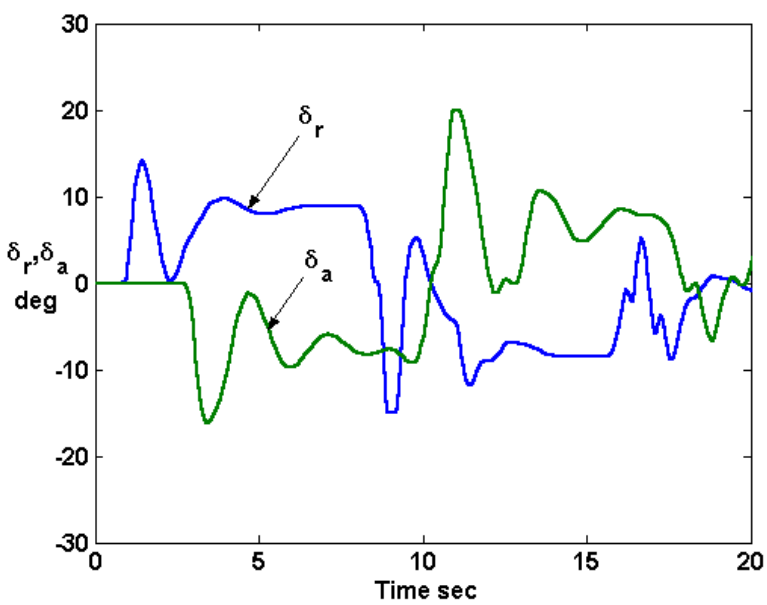

FIGURE 22. AILERON AND RUDDER INPUTS FOR TRACKING FIGURE 21

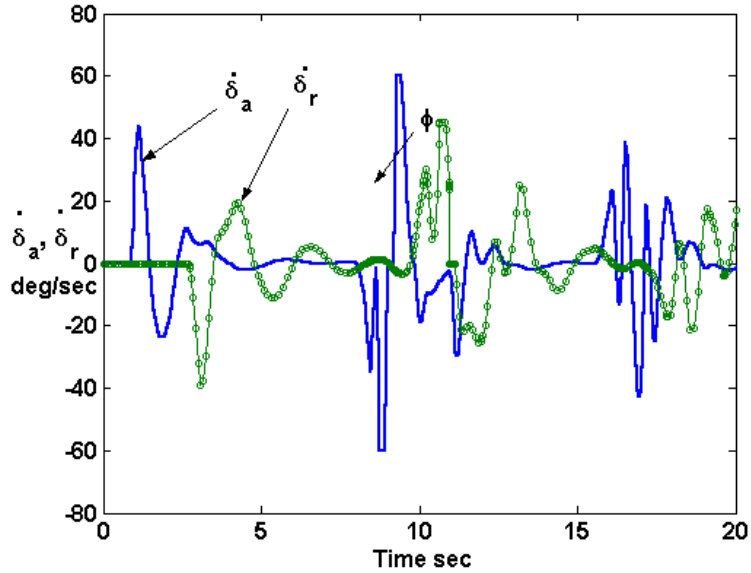

FIGURE 23. AILERON AND RUDDER RATES FOR TRACKING FIGURE 21

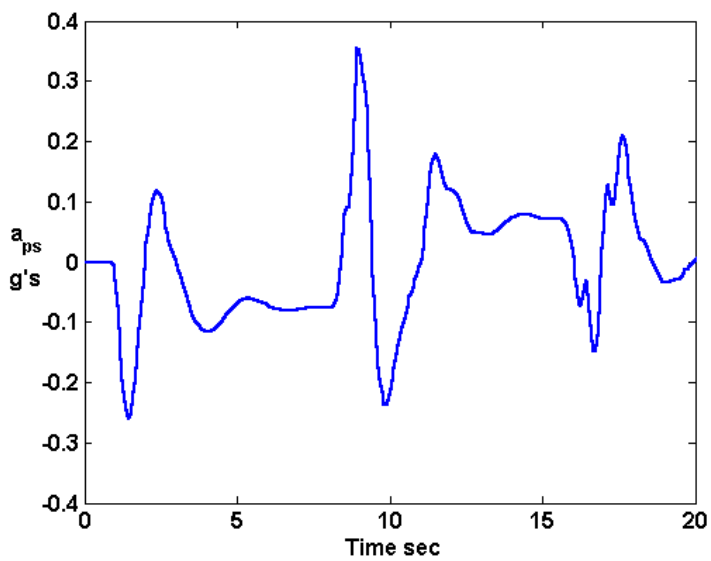

FIGURE 24. LATERAL ACCELERATION IN THE COCKPIT FOR TRACKING FIGURE 21

Increasing the sensitivity of the rudder system to high level resulted in incipient instability in the pilot/vehicle system. Lateral accelerations at the PS exceeded 0.5 g's in one excursion. Again, such values are likely to serve as a triggering event for a PIO. Creating regressive behavior in the pilot model in both the roll and sideslip channels leads to the PIO shown in figure 25. The PIO frequency is approximately 2.9 rad/sec or 0.46 Hz. Again, significant amplitude and rate limiting are evident in the figure.

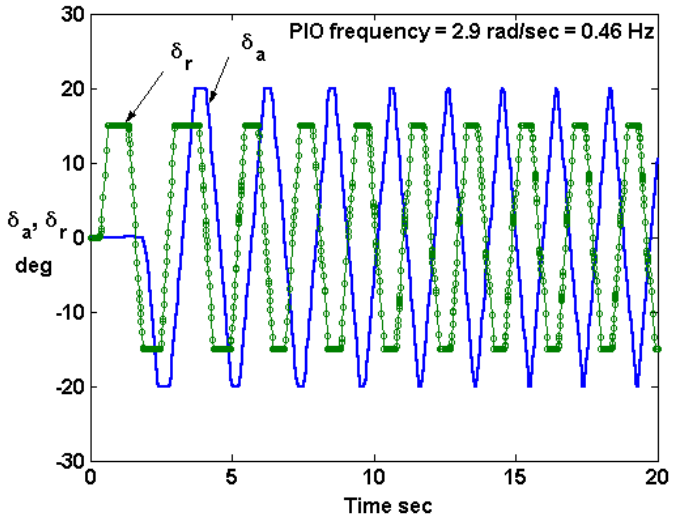

FIGURE 25. RUDDER AND AILERON INPUTS IN SIMULATED PIO WITH PILOT MODEL ADOPTING REGRESSIVE BEHAVIOR (PIO frequency 2.9 rad/sec)

1.4 SUGGESTIONS FOR FLIGHT SIMULATOR INVESTIGATIONS.

Compared to those for wheel and column, rudder force/feel system designs have received little attention in the literature [13]. However, recent accidents, such as American Airlines flight 587 and other rudder-related incidents with transport aircraft [14], have uncovered a need for firm design requirements for these systems. Given the inherent dangers of flight testing in which the possibility of excessive vertical stabilizer loading can easily occur, it would appear that ground-based flight simulators offer the most practical means for delineating acceptable force/feel characteristics. It is essential in defining the tasks that would be performed in such investigations that the recommendations of reference 15 be recalled. Specifically, any tasks selected for discerning the PIO susceptibility of force/feel system characteristics need to be sufficiently challenging and aggressive. The coordinated roll attitude capture and wings-level sideslip captures exercised herein via computer simulation may serve as two such tasks. This and other candidate tasks could undergo preliminary evaluation on simple desktop engineering simulators to assess their worth and practicality. One such investigation is discussed in section 2.

1.5 SUMMARY OF SECTION 1.

The research described in this section has used a simple dynamic model of the lateral/directional dynamics of a transport aircraft. A system survey of possible manual loop closures was presented. Using a Structural Model of the human pilot, two tracking tasks were examined, each with an eye toward capturing possible pilot/vehicle behavior than could occur in large roll upsets and in deliberate sideslip excursions. The pilot model was extended to emulate the effects of control sensitivity. The coordinated use of aileron and rudder inputs for roll attitude tracking was shown to exhibit poor performance and stability compared to aileron inputs alone. In addition, it was suggested that rudder force/feel systems with large sensitivities (low force

gradients) could precipitate lateral/directional PIOs with such coordinated strategies due to the large lateral accelerations at the PS that occurred. The sideslip capture task also suggested that large control sensitivities in the rudder control system could also lead to large lateral accelerations at the PS that could serve as a PIO trigger. Although simplified in nature, the analytical study emphasized the handling qualities and performance issues that can arise in continuous use of rudder inputs in flight control tasks.

2. DESKTOP SIMULATION.

2.1 INTRODUCTION.

A desktop, human-in-the-loop simulation of the vehicle and tasks described in section 1 was conducted. The simulation itself used a simulation software package HPESIM from High Plains Engineering [16]. This package allows pilot-in-the-loop, five or six degree-of-freedom simulation of aircraft dynamics. A variety of visual scene representations are possible. Here, a head-up display was employed and will be described in the following. The simulation is nonlinear in nature, although linear stability derivatives provide the vehicle model. Nonlinearities arise since no small angle approximations are employed in solving the equations of motion, and actuator amplitude and rate limiting can be modeled.

2.2 VISUAL SCENE REPRESENTATION.

Figure 26 shows the visual scene representation used herein. The small aircraft symbol at the center of the display is a flight path symbol that was used in the sideslip capture task but was removed for the large roll attitude change task. For the two tasks discussed in section 1, a clear plastic overlay was placed over the terminal, as shown in figure 27.

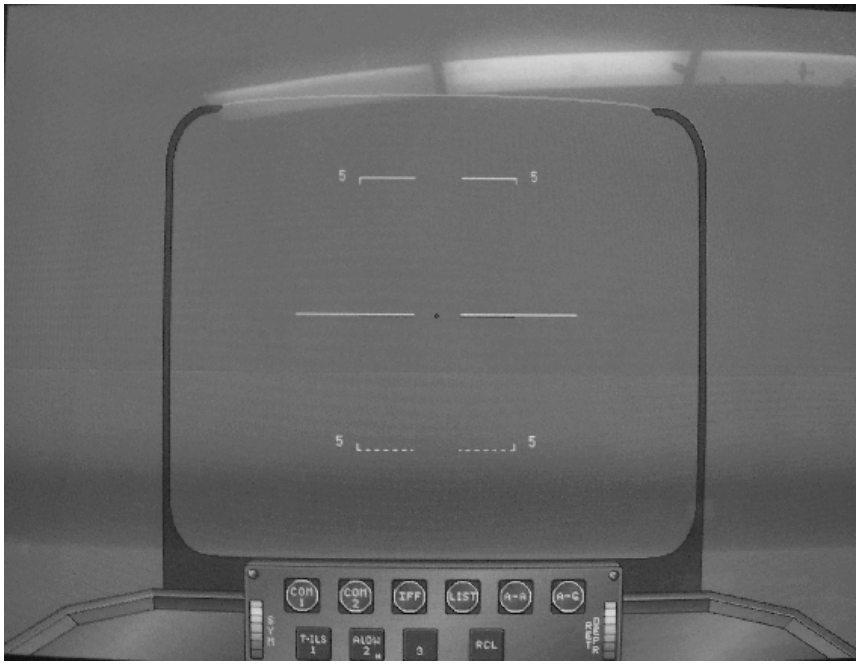

FIGURE 26. VISUAL SCENE REPRESENTATION IN DESKTOP SIMULATION

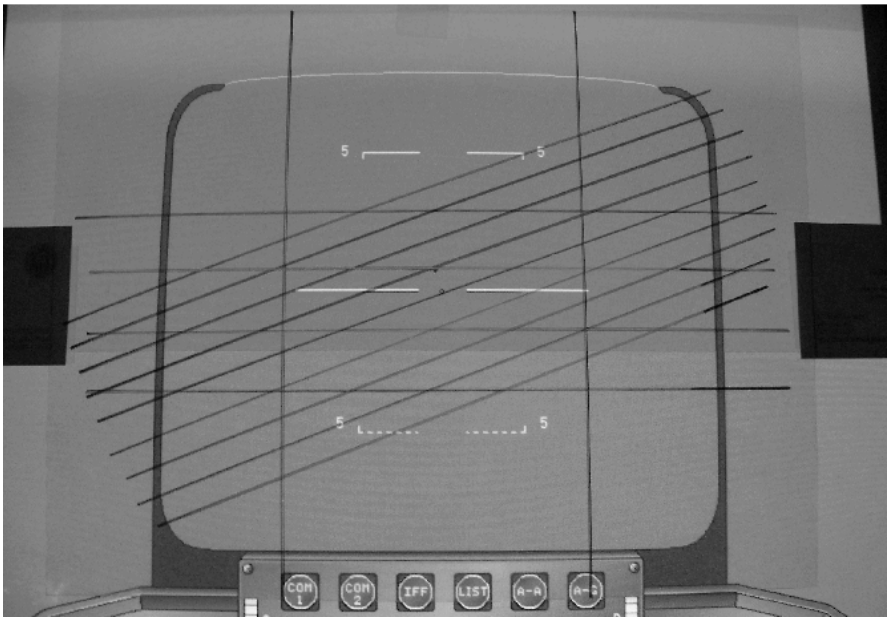

FIGURE 27. VISUAL SCENE REPRESENTATION WITH PLASTIC OVERLAY

The slanted lines in figure 27 represent 20° roll attitudes (the magnitude of the commands used in task 1 in section 1). The two vertical lines represent 5° sideslip excursions (the magnitude of the sideslip commands used in task 2 in section 1). The nominal eye-to-display distance for the simulations was 26 inches. The monitor size was 14.4375 by 10.875 in. HPESIM uses the monitor size to create a vertical field of view in the visual scene.

2.3 INCEPTOR.

Figure 28 shows the subject's chair and the inceptor used in the simulation. The joystick shown allowed three-axis control. The desk shown in figure 28 allowed arm support during the tracking tasks. Aileron inputs were created by lateral stick deflection, with rudder inputs created by rotating the stick about a vertical axis. When viewed from above, a clockwise rotation of the joystick was equivalent to the right pedal being depressed. The desktop version of HPESIM requires inputs from a single joystick, thus separate pedals to provide rudder inputs could not be accommodated. Though not employed in the tasks examined here, elevator inputs were possible through longitudinal stick deflection. The inceptor incorporated a light return spring in all axes. To approximate the dynamics of the force/feel systems of equations 18 and 19, filters in the form of the transfer functions given by these equations were implemented in software in HPESIM. Of course, proprioceptive feedback reflecting these dynamics were not available to the subject. Displacement thresholds for wheel and pedal inputs were 20% and 10% of full deflections, respectively, again created in software. Although longitudinal aircraft dynamics were included in the simulation, no column inputs were allowed. The natural aircraft short-period and phugoid motions were mitigated by creating a high-gain, pitch-attitude stability augmentation system to be described.

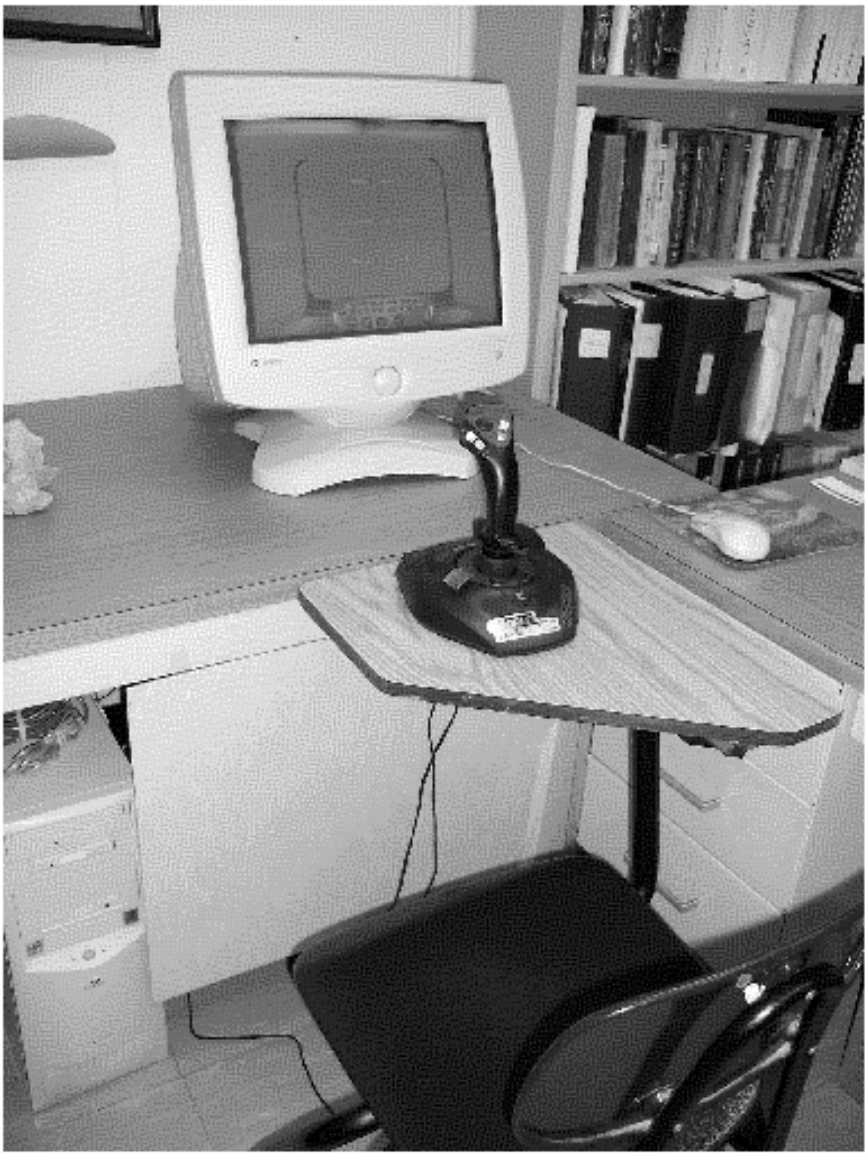

FIGURE 28. PHYSICAL SIMULATION SETUP

2.4 AERODYNAMIC MODEL.

As in section 1, the aerodynamic model employed in the simulation was taken from reference 5 and represented a DC-8 aircraft with stability derivatives defined for flight condition 8002, corresponding to an airspeed of 468.2 ft/sec and an altitude of 15,000 ft. The stability derivatives in reference 5 are referred to as a stability axis system, whereas HPESIM requires a body-axis system, with the x-body axis aligned with the mean aerodynamic chord. To transform the derivatives from stability to body axes, the trim angle of attack is required. This information was not provided in reference 5, therefore, a trim angle of attack of 5° was estimated here.

2.5 CONTROL LAW IMPLEMENTATION.

Figures 29 and 30 show the general format available in HPESIM for setting up simulation details and for implementing control laws (shown for the longitudinal axis).

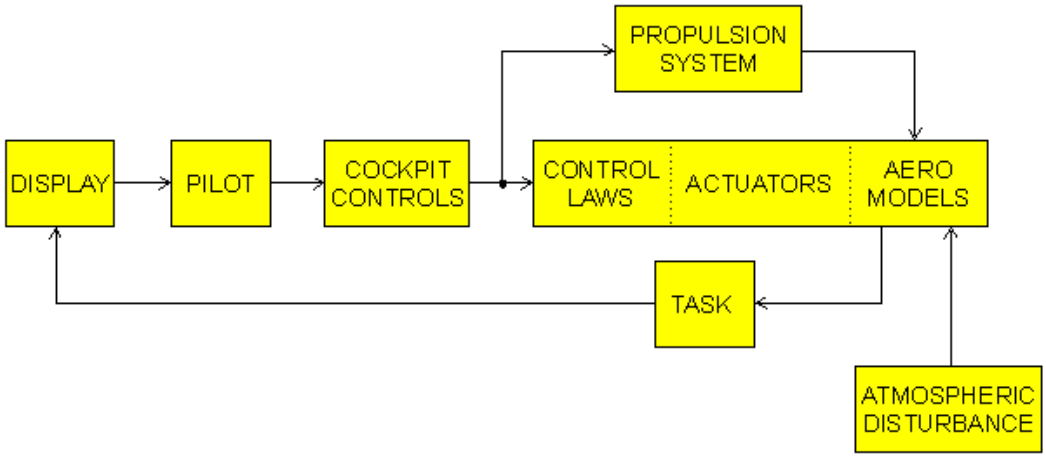

FIGURE 29. SIMULATION DETAILS IN HPESIM

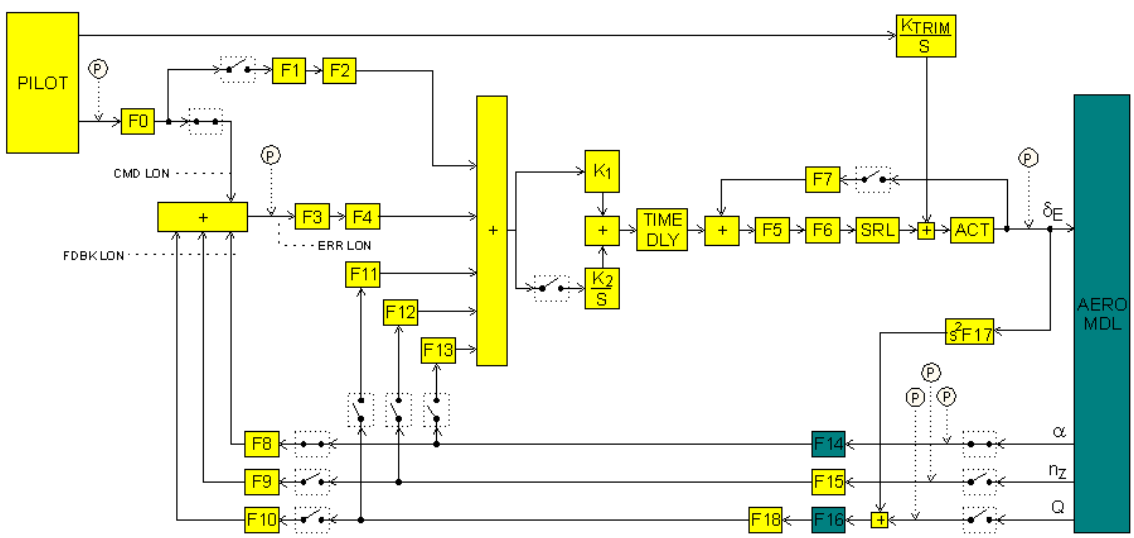

FIGURE 30. CONTROL LAW IMPLEMENTATION SCHEME IN HPESIM (LONGITUDINAL AXIS SHOWN)

As mentioned in the preceding, a longitudinal SAS was designed to reduce the pitch attitude deviations in the vehicle. The SAS was defined as

$$\frac{\delta_e}{\theta}(s) = 5(s+1) \;\; rad/rad \tag{20}$$

A yaw damper similar to that used in the analysis of section 1 was also implemented in the lateral directional axis. Because of the default transfer function forms available in HPESIM, this yaw damper took the form

$$\frac{\delta_r}{r}(s) = \frac{114[0.99,0.01]}{[0.99,0.5]} \; rad/rad/sec \tag{21}$$

This can be compared to equation 6 in section 1. No pure differentiation elements (s) were available in HPESIM, and only second-order numerator and denominator forms could be accessed. The form of equation 21 exhibits small amplitudes at low frequency (below 0.5 rad/sec) and a constant amplitude of 2.28 for frequencies beyond 0.5 rad/sec, as does the transfer function of equation 6.

2.6 TEST SUBJECT.

The author served as the test subject in this simulation. It must be emphasized that this simulation effort was an initial, exploratory effort aimed at a qualitative evaluation of the analytical results of section 1 and an assessment of possible tasks to be evaluated in other, more realistic simulation studies. For these reasons, no other test subjects were sought.

2.7 SIMULATION RESULTS.

2.7.1 Task 1: Large Roll Attitude Change.

Figure 31 shows a 20° roll attitude change and corresponds to figure 11 with $K_r = 0$. Figure 32 shows the aileron and rudder inputs that produced this response. Two points should be noted in figure 32. First, no amplitude limiting is actually occurring in the aileron input for this task. The flat portions of the input are due to signal quantization created by the joystick. Second, just as in the computer simulation of figure 12, the small rudder inputs are attributable to the action of the yaw damper, not to any inputs provided by the subject through the joystick.

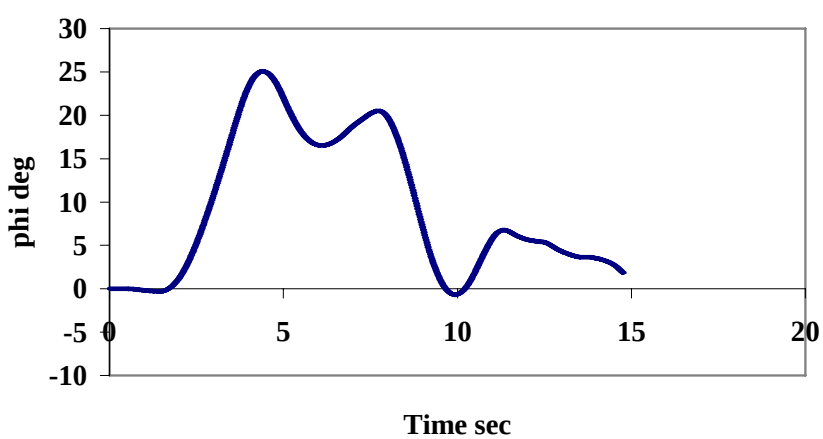

FIGURE 31. LARGE ROLL ATTITUDE CHANGE TASK, WHEEL ONLY SUBJECT INPUTS

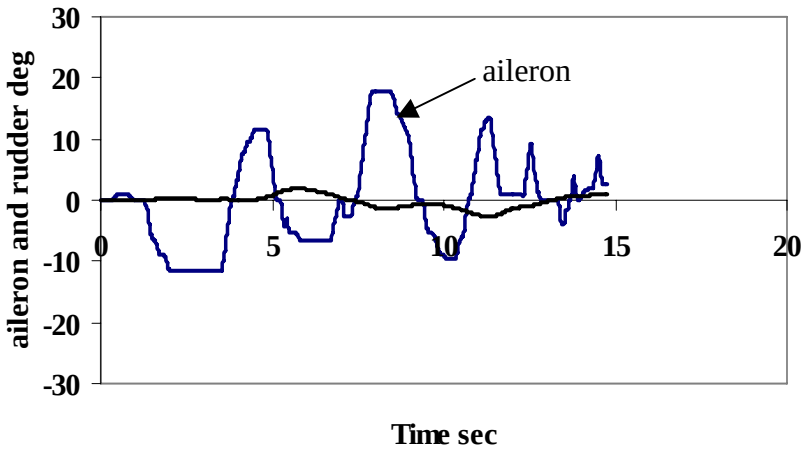

FIGURE 32. AILERON AND RUDDER INPUTS FOR TASK OF FIGURE 31

Figure 33 shows aileron and rudder rates for this task indicating significant aileron rate saturation occurring. Again, this result is similar to the computer simulation result shown in figure 13.

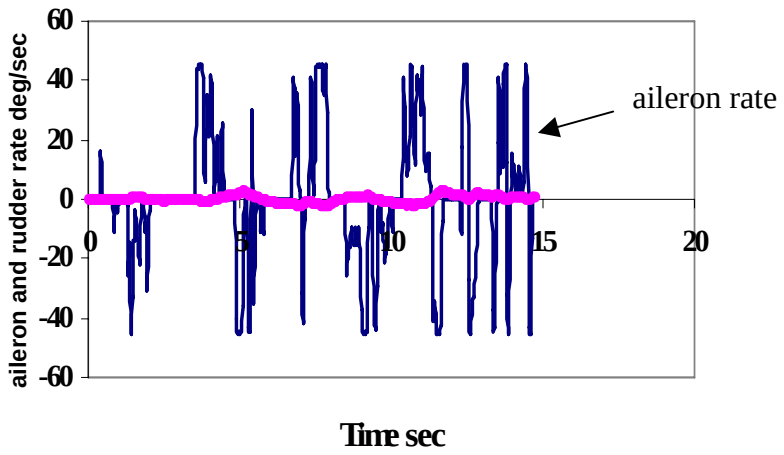

FIGURE 33. AILERON AND RUDDER RATES FOR TASK OF FIGURE 31

Figure 34 shows a 20° roll attitude change, including both wheel and pedal inputs. As opposed to the computer simulation study of section 1, no specific K_r value can be identified in this human-in-the-loop study. Nonetheless, incipient instability is evident in figure 34 much as was the case in figure 11 with K_r = 0.75. As in figure 11, the frequency of oscillation apparent in figure 34 is very near that of the dutch roll mode for this aircraft and flight condition. Figure 35 shows the aileron and rudder inputs for this task, with figure 36 showing rates. Some aileron rate limiting is evident, and again, no amplitude limiting is occurring in figure 35 as the flat portions of the input are due to signal quantization created by the joystick.

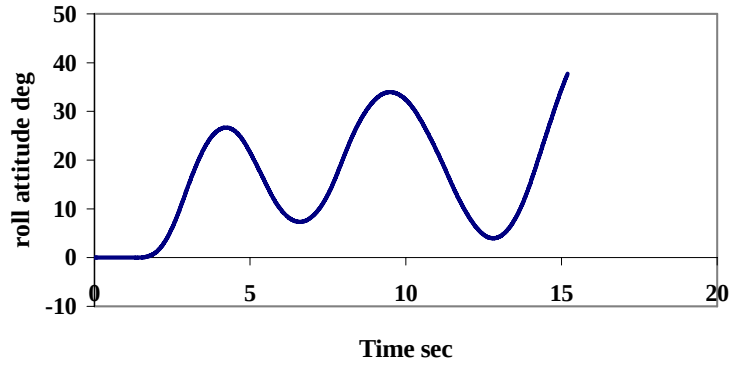

FIGURE 34. LARGE ROLL ATTITUDE CHANGE TASK, WHEEL AND PEDAL INPUTS

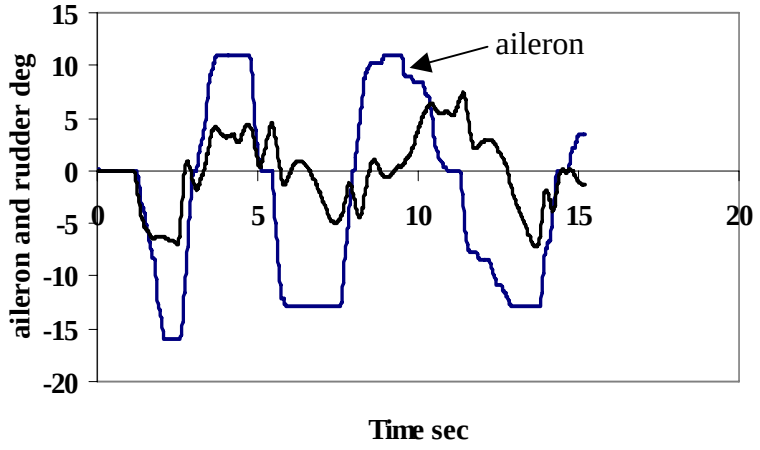

FIGURE 35. AILERON AND RUDDER INPUTS FOR TASK OF FIGURE 34

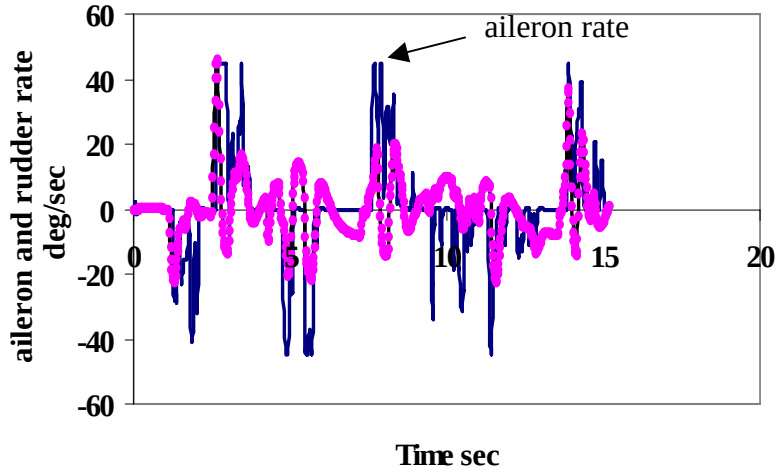

FIGURE 36. AILERON AND RUDDER RATES FOR TASK OF FIGURE 34

Figure 37 compares the lateral acceleration at the pilot's station (a_{ps}) for the tasks of figures 31 and 34. Not surprisingly, the large roll attitude change task with both wheel and pedal inputs resulted in considerably larger accelerations than were obtained with just wheel inputs alone.

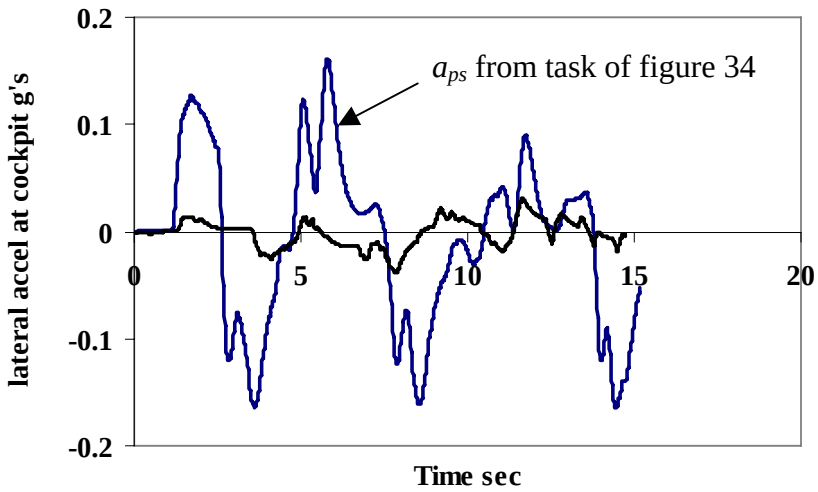

FIGURE 37. COMPARISON OF LATERAL ACCELERATION AT PILOT'S STATION (a_{ps}) FOR TASKS OF FIGURES 31 AND 34

Figure 38 shows the large roll attitude change task with both wheel and pedal inputs now deliberately performed with a low-gain tracking approach. Figures 39 and 40 show the aileron and rudder inputs and rates, respectively, for this low-gain tracking. As predicted by the bandwidth and phase delay results of table 1, low-gain behavior (low bandwidth) is required for stable performance when both wheel and pedal inputs are used in the large roll attitude change task.

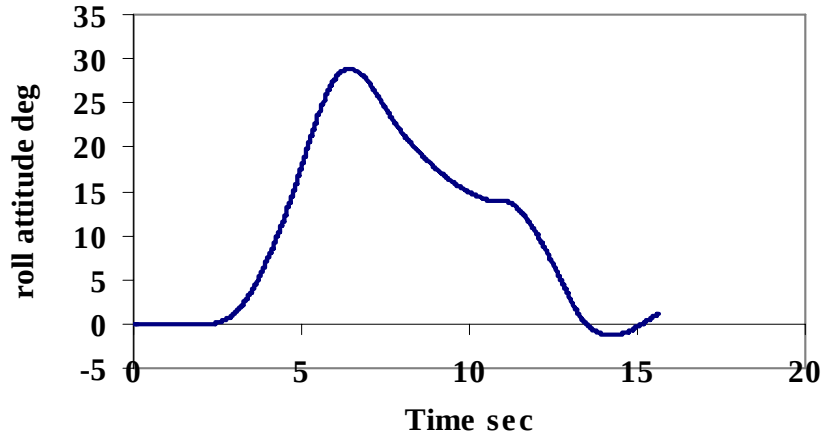

FIGURE 38. LARGE ROLL ATTITUDE CHANGE TASK, WHEEL AND PEDAL INPUTS, PERFORMED WITH LOW-GAIN TRACKING BEHAVIOR

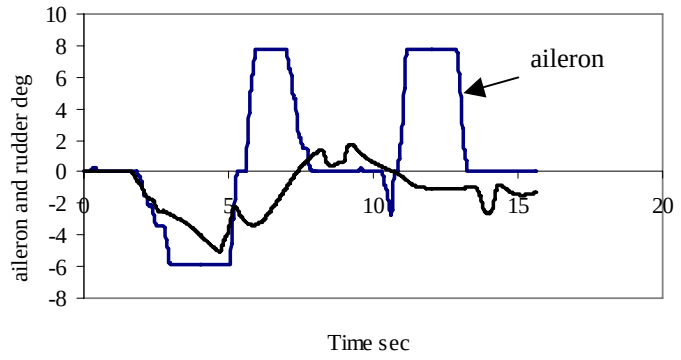

FIGURE 39. AILERON AND RUDDER INPUTS FOR TASK OF FIGURE 38

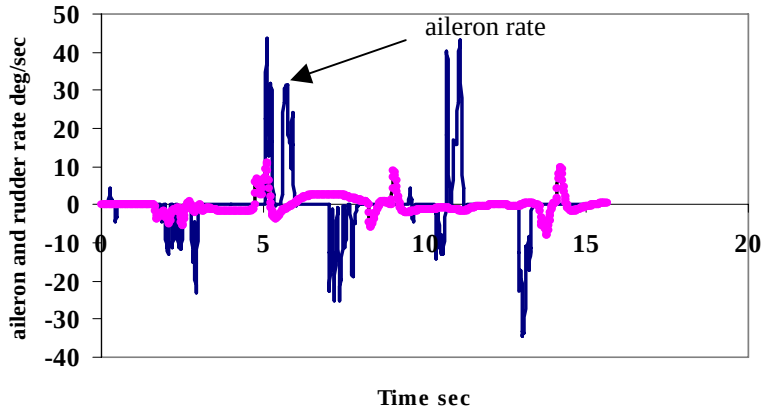

FIGURE 40. AILERON AND RUDDER RATES FOR TASK OF FIGURE 38

A final alternative tracking strategy for the large roll attitude change task can be considered, namely, one in which rudder inputs are employed but only in transient fashion. That is, rudder inputs are brought in to initiate and arrest roll motions, but are not applied in continuous fashion, i.e., closed-loop tracking with rudder is not employed. Figures 41 through 43 summarize simulation results for this strategy. The performance shown here is qualitatively superior to any of the previous results.

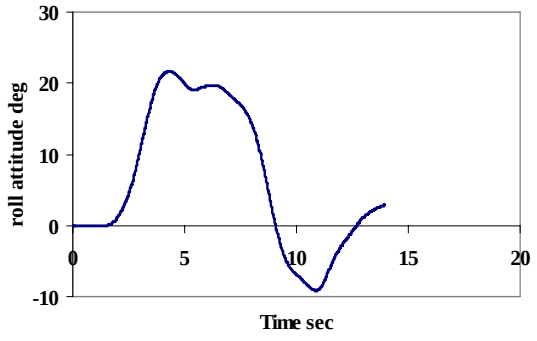

FIGURE 41. LARGE ROLL ATTITUDE CHANGE TASK, WHEEL AND PEDAL INPUTS, PERFORMED WITH TRANSIENT RUDDER INPUTS

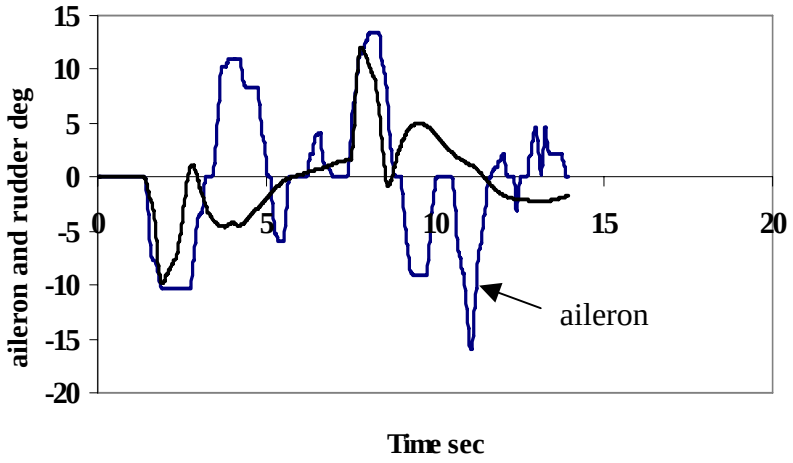

FIGURE 42. AILERON AND RUDDER INPUTS FOR TASK OF FIGURE 41

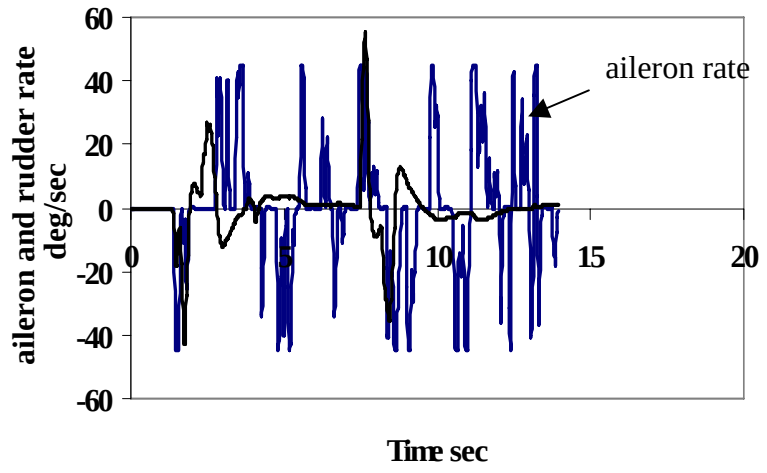

FIGURE 43. AILERON AND RUDDER RATES FOR TASK OF FIGURE 38

2.7.2 Task 2: Wings-Level Sideslip Captures.

Figure 44 shows the sideslip response to an attempt at ±5° sideslip captures. The term wings level refers to the desired task performance, and not that actually obtained just as was the case in the computer simulation of section 1. The subject found this task very difficult, as the roll attitude excursions evident in figure 44 indicate. Part of the difficulty may be attributable to the nature of the control inceptor, i.e., both wheel and pedal inputs are created with the joystick rather than with an actual wheel and pedals. Nonetheless, the subject found the transition from +5° to -5° very challenging. The roll attitude excursions are very large in the latter part of the maneuver where the -5° sideslip is being attempted. Figures 45 and 46 show the aileron and rudder inputs and their rates. Note that significant aileron rate limiting is occurring in the task.

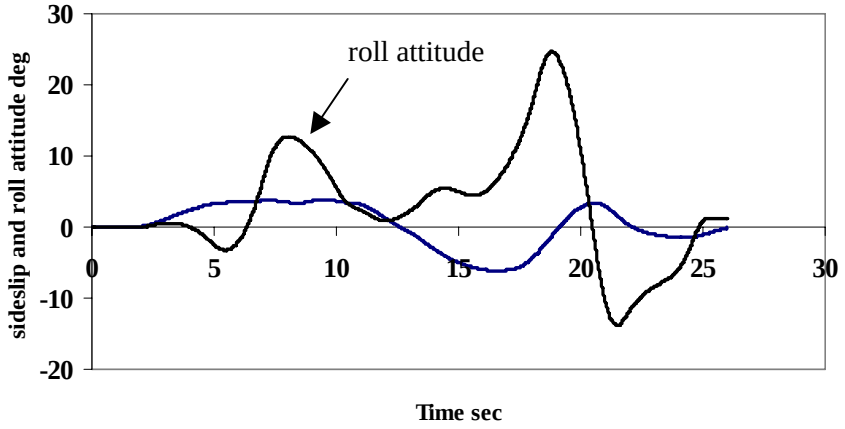

FIGURE 44. SIDESLIP AND ROLL ATTITUDE IN SIDESLIP CAPTURE TASK

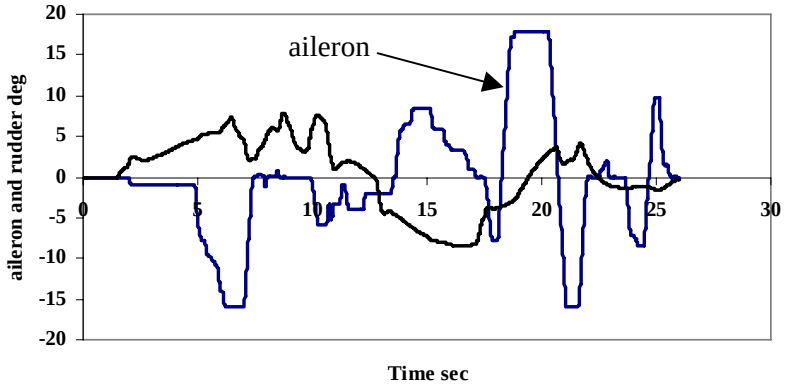

FIGURE 45. AILERON AND RUDDER INPUTS FOR TASK OF FIGURE 44

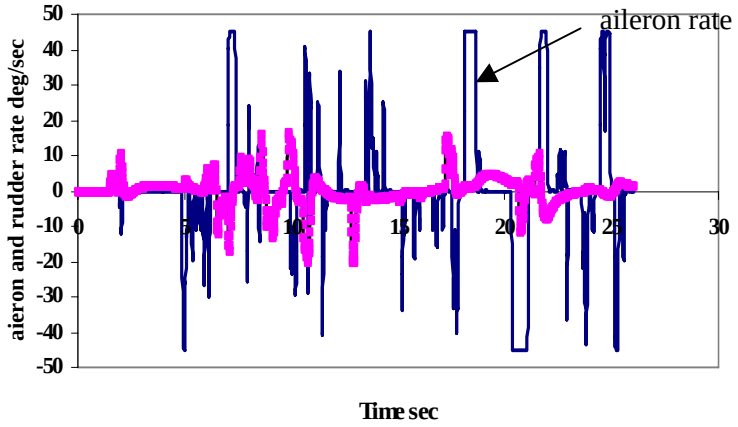

FIGURE 46. AILERON AND RUDDER RATES FOR TASK OF FIGURE 44

A much more reasonable task can be defined by requiring a wings-level sideslip capture of +5°, followed by a return to 0° sideslip and wings level. The results of employing this approach are shown in figures 47 through 49. For ease of comparison, figures 47 through 49 have been scaled identically to figures 44 through 46.

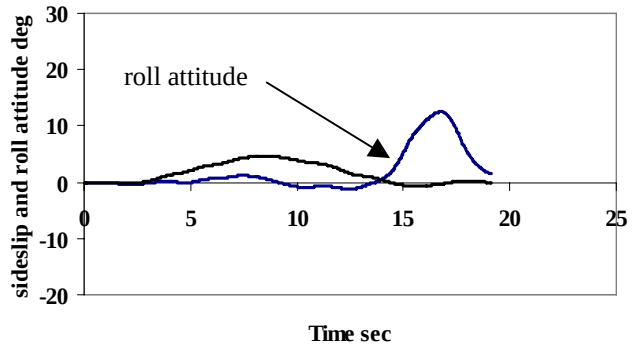

FIGURE 47. MODIFIED SIDESLIP CAPTURE TASK

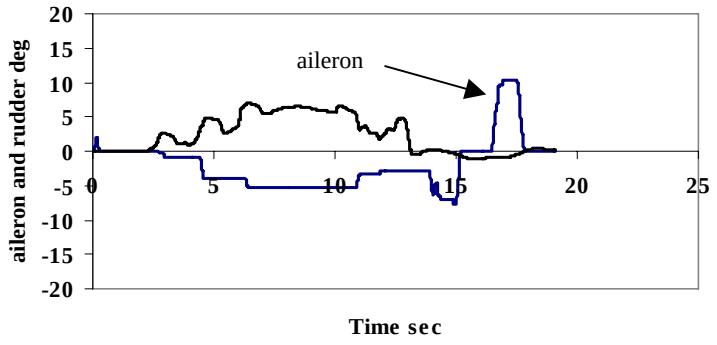

FIGURE 48. AILERON AND RUDDER INPUTS FOR TASK OF FIGURE 47

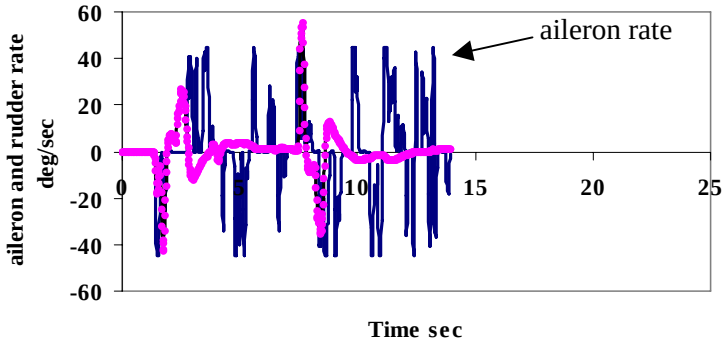

FIGURE 49. AILERON AND RUDDER RATES FOR TASK OF FIGURE 47

An additional experiment was conducted to evaluate the effect of rudder sensitivity. Here, the displacement threshold for the pedal was increased from 25% to 50% of full deflection[2] and the sensitivity of the pedal was tripled. With these values, the subject could not successfully complete any wings-level sideslip captures. Particularly noticeable was the reverse action of the rudder inputs, wherein an attempt to capture a +5° sideslip angle with pedal inputs initially induced a negative (left wing down) roll response. This reverse action is attributable to the nonminimum phase zero in the transfer function $\frac{\beta}{\delta_r}(s)$ and was touched upon in section 1 of the report.

2.8 SUMMARY OF SECTION 2.

The research summarized in this section has served as a preliminary and exploratory human-in-the-loop desktop simulation of the vehicle and tasks analyzed in section 1. The simulation effort has qualitatively evaluated the analytical results of section 1. The handling qualities and potential flight safety problems of high-gain, closed-loop tracking using coordinated aileron and rudder inputs that were suggested in section 1 have also appeared in the simulation. The use of wings-level sideslip captures as an evaluation maneuver warrants further investigation.

3. PEDAL FORCE/FEEL SYSTEM COMPARISON.

3.1 INTRODUCTION.

The graphs in figures 50 through 52 show three comparisons of three transport aircraft pedal force/feel systems and a helicopter. The helicopter was the UH-60A Blackhawk, and the transport aircraft were the Airbus A300-600 at 240 kts, the Boeing 767, and the Airbus A300-B2-B4. The Airbus A300-B2-B4 was the immediate predecessor of the A300-600 and is very similar in size, weight, and configuration. The Blackhawk data were obtained from the research staff at the Army Aeroflightdynamics Directorate at NASA Ames. The A300-600, A300-B2-B4, and B-767 data were obtained as part of a report on the American Airlines Flight 587 accident. These plots involve straight-line approximations to the force/displacement characteristics with full control movement, with no cable stretch involved. It should be mentioned that, as opposed to the A300-600 and UH-60A data, the B-767 and A300-B2-B4 characteristics were obtained from tabular data that did not give specific force/feel characteristics within the breakout area. It should be noted that, as used here, maximum force is defined as the pedal force that yields a maximum pedal displacement without inducing cable stretch in the mechanical system. As shown, larger forces can be applied to the force/feel system. Finally, it is important to emphasize that the force/feel characteristics for the pedal system of the A300-600 are a function of airspeed. This is the reason for associating the particular data for this vehicle with the 240-kt airspeed. This is not the case for the UH-60A, A300-B2-B4, and B-767 vehicles, where the force/feel pedal characteristics are invariant with airspeed. Like the B-767, the A300-B2-B4 rudder system is a ratio system, whereas the A300-600 is a variable stop system.

[2] It is important to recall that this threshold is a software threshold and is not reflected in the force/displacement characteristics of the joystick.

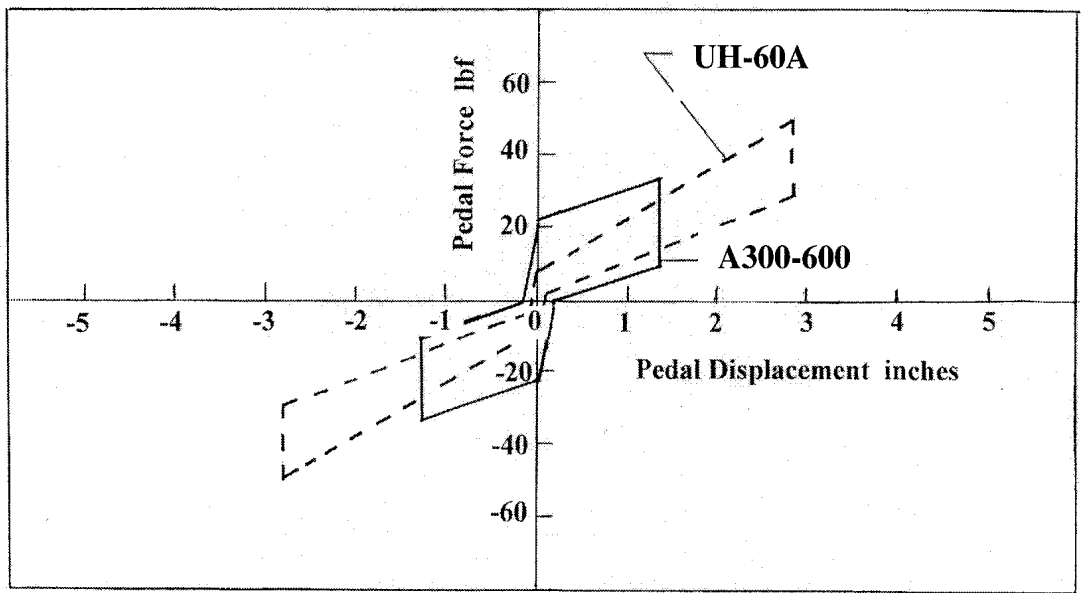

FIGURE 50. PEDAL FORCE/FEEL SYSTEM COMPARISON OF THE A300-600 AT 240 kts AND THE UH-60A BLACKHAWK HELICOPTER

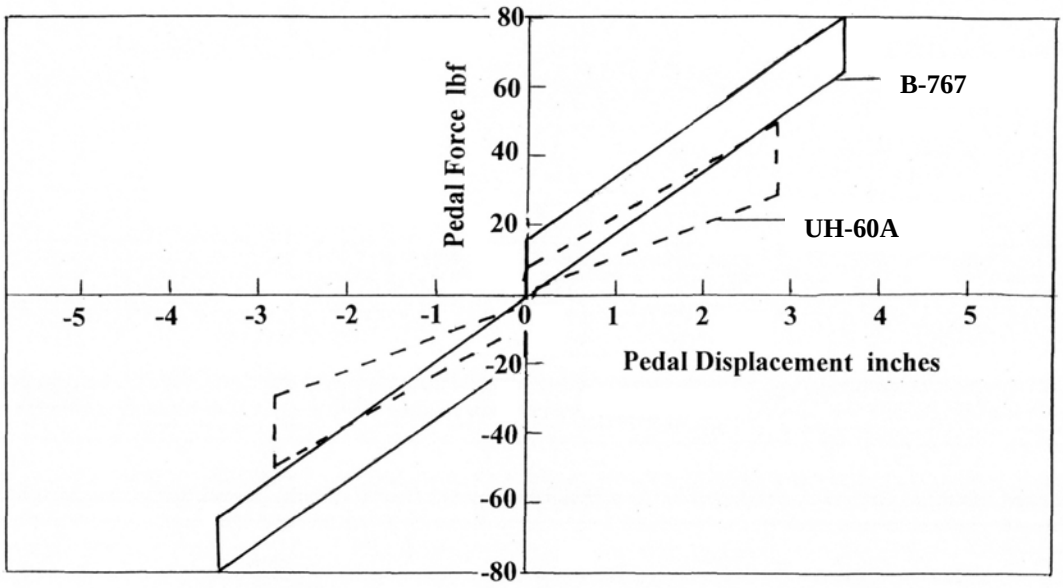

FIGURE 51. PEDAL FORCE/FEEL SYSTEM COMPARISON OF THE B-767 AND THE UH-60A BLACKHAWK HELICOPTER

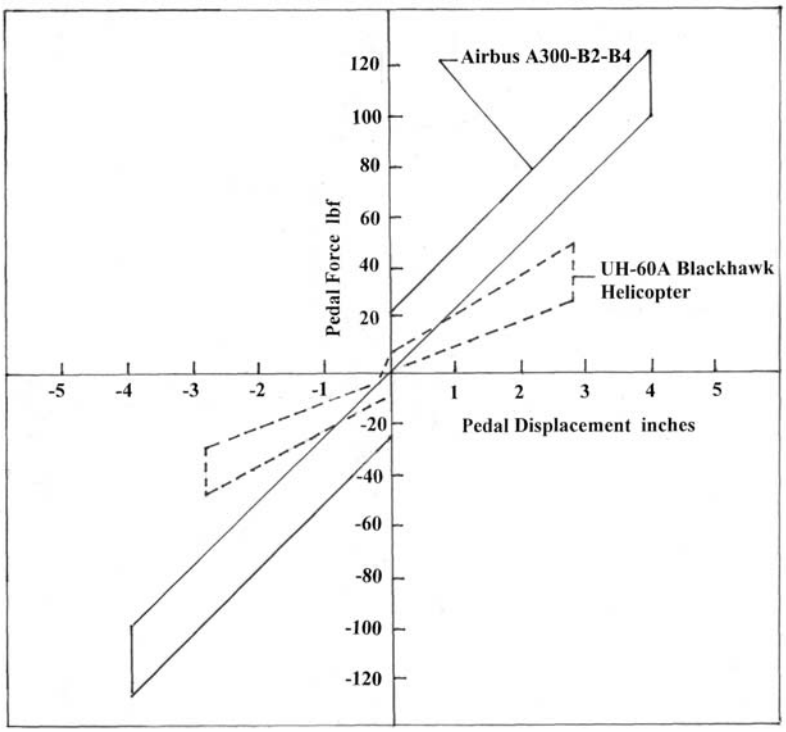

FIGURE 52. PEDAL FORCE/FEEL SYSTEM COMPARISON OF THE AIRBUS A300-B2-B4 AND THE UH-60A BLACKHAWK HELICOPTER

3.2 THE HELICOPTER COMPARISON.

The primary reason for choosing a military rotorcraft for a benchmark case was that the vehicles can, and do, perform tasks in which precise heading/yaw rate control is obtained with pedal inputs. UH-60A flight tests are routinely conducted at NASA Ames that involve maneuvers from ADS-33E [17] in which precise heading control was required, e.g., reference 18. These maneuvers consist of hovering turns, pirouettes, lateral repositions, and sidesteps in which heading performance requirements are spelled out in a quantitative fashion [17]. Of course desirable handling qualities and task performance depend on more than just the characteristics of the force/feel system. However, acceptable force/feel system characteristics constitute a necessary condition for achieving these. Thus, the nature of the pedal force/feel system on the UH-60A is more than just a passing interest.

3.3 COMPARING PEDAL FORCE/FEEL CHARACTERISTICS.

Figures 50 through 52 clearly indicate significant differences between the pedal force/feel system on the A33.00-600 at 240 kts and those for the UH-60A, B-767, and A300-B2-B4. For the reason stated in the preceding paragraph, the common system selected for comparison in each figure is the UH-60A. The differences are summarized in table 2. In addition to the quantitative differences, it is apparent from the graphs that the system for the A300-600 at 240 kts is significantly more nonlinear than the UH-60A, B-767, and A300-B2-B4. The differences between the A300-600 and A300-B2-B4 force/feel characteristics are particularly noteworthy,

not only for their force/displacement characteristics (compare the solid lines in figures 50 and 52) but also because these two aircraft are nearly identical in size, weight, and general aerodynamic configuration.

TABLE 2. FORCE/FEEL SYSTEM SUMMARY

Vehicle	Ratio of Maximum Force to Breakout Force	Maximum Force (lbf)	Maximum Displacement (in.)
UH-60A	5.7	50	2.8
B-767	4.71	80	3.6
A300-B2-B4	5.7	125	4.0
A300-600*	1.45	32	1.3

*240-kt airspeed

The graphs invite the following question: Is the linearity of the force/displacement characteristics of the control inceptor, in this case the pedals, a useful metric for acceptability of these devices? Linearity is meant to be the ability of the pilot to minimize the nonlinear characteristics when precise control is involved, such as in tracking or disturbance regulation. The primary means by which this linearization occurs is through gain regulation by the pilot.

3.4 A COMPUTER SIMULATION.

The system in figure 53 represents a simplified pilot/vehicle system with a nonlinear force/feel system. Although the symbol for roll attitude (phi) was identified as the system input and output, the symbol was used merely for convenience here. Figure 53 represents any generic tracking task in which force/feel characteristics can be compared.

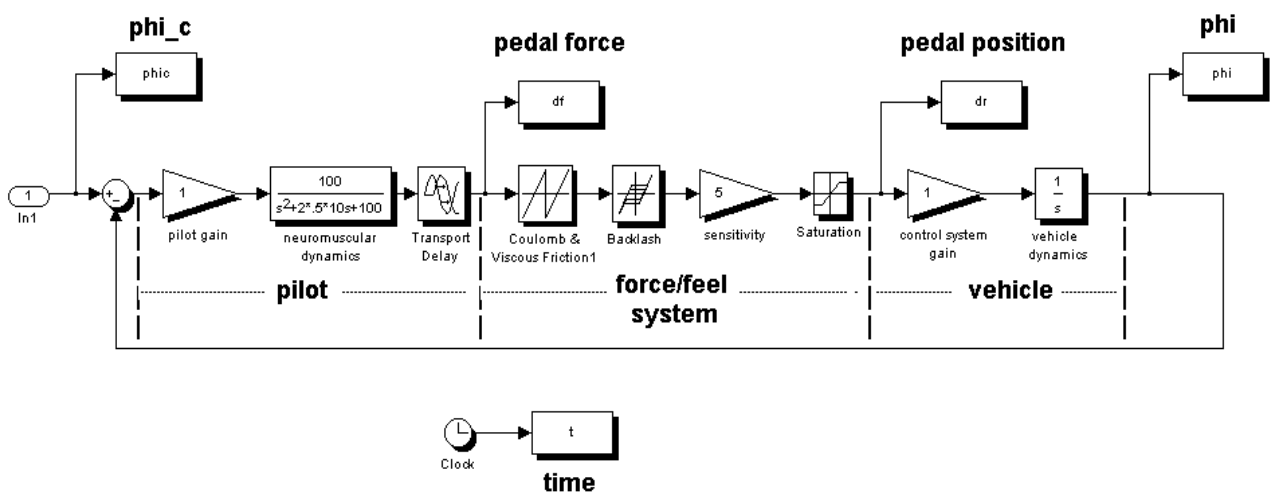

FIGURE 53. A SIMPLIFIED COMPUTER MODEL OF THE PILOT/VEHICLE SYSTEM

The pilot in figure 53 consists of a gain, a second-order transfer function modeling neuromuscular dynamics, and a 0.2-second time delay. This pilot model is considerably simpler than the Structural Model of the pilot offered in section 1. The vehicle is a simple integrator with an adjustable control system gain. By considering the product of the transfer functions of the pilot, force/feel system, and vehicle, it can be shown that the open loop/pilot vehicle system obeys the dictates of the Crossover Model of the human pilot [9]. Two force/feel systems will be considered. These systems correspond approximately to the systems on the A300-600 and A300-B2-B4 (shown in figures 50 and 52) and are referred to here as System A and System B. In this simulation, each of the force/feel systems will be capable of the same maximum amplitude command to the integrator (vehicle model) through the appropriate adjustment of the control system gain shown in figure 53. Figure 54 shows the force/displacement curves for systems A and B in the simulation. Note that in this simulation, the absolute magnitude of the forces and displacements involved are of no concern, therefore, no units are attached to the axis definitions in figure 54.

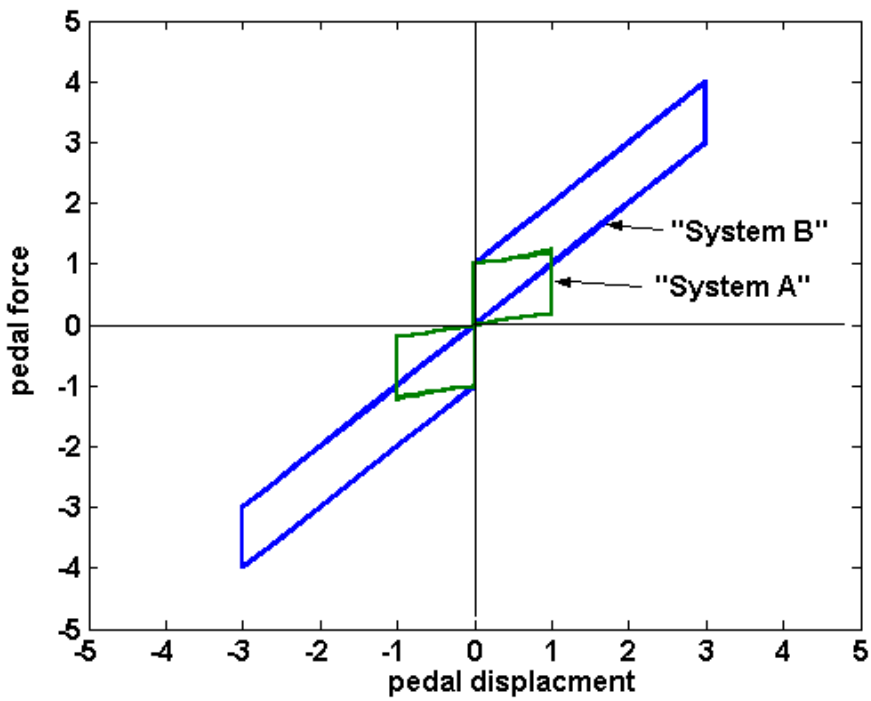

FIGURE 54. REPRESENTATION OF THE PEDAL FORCE/FEEL SYSTEMS A AND B IN THE COMPUTER SIMULATION OF FIGURE 53

A 5-second pulsive roll command was provided in the simulation. The units involved here are not important, given the simplified nature of the simulation. Figures 55 and 56 show the responses when systems A and B are used for the pilot gains K_p = 1, 2, 4, 6. As can be clearly seen from figure 55, responses of the high-sensitivity System A is much less predictable and is much more sensitive to the particular pilot gain chosen. Oscillations are apparent for all pilot gains at or above K_p = 4, whereas no such oscillations appear in figure 56 for System B. The inability of either system to respond with K_p = 1 is merely due to the fact that this gain value was not large enough to overcome the identical breakout forces in either force/feel system.

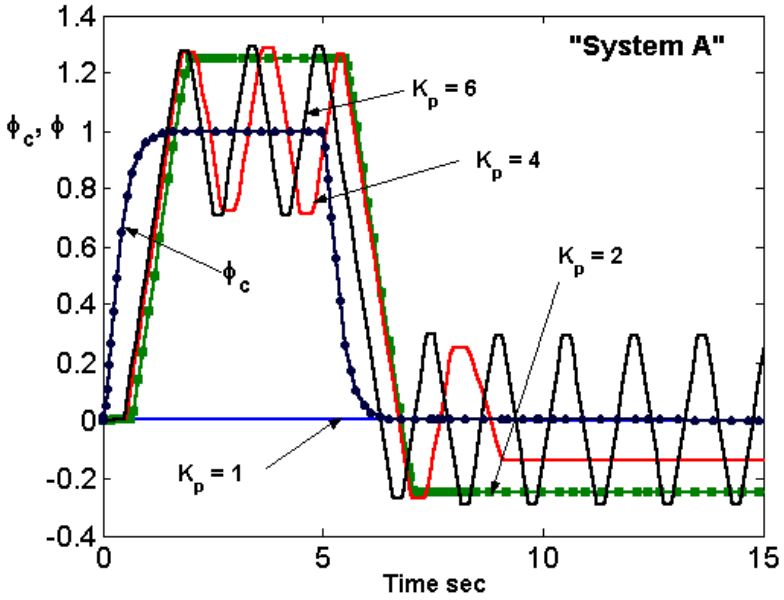

FIGURE 55. RESPONSES OF THE COMPUTER SIMULATION SYSTEM OF FIGURE 53 FOR DIFFERENT PILOT GAINS FOR THE SYSTEM A PEDAL FORCE/FEEL SYSTEM

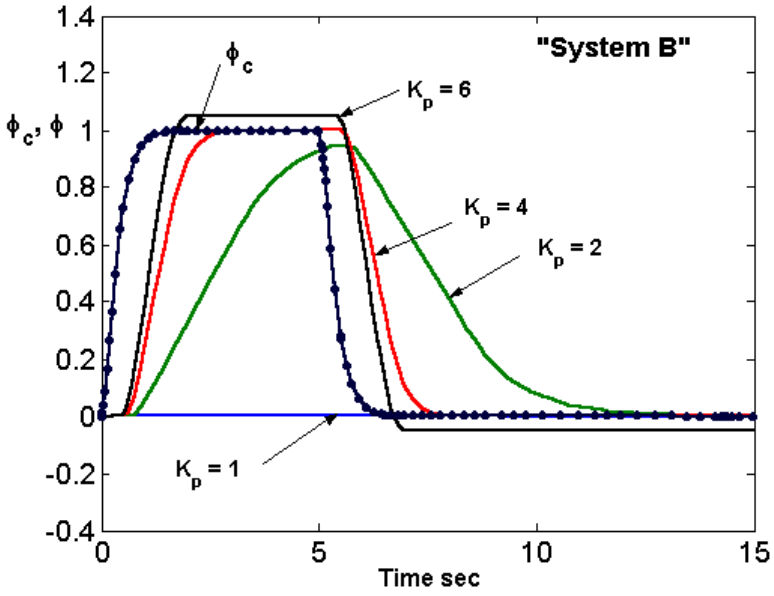

FIGURE 56. RESPONSES OF THE COMPUTER SIMULATION SYSTEM OF FIGURE 53, FOR DIFFERENT PILOT GAINS FOR SYSTEM B PEDAL FORCE/FEEL SYSTEM

Figure 57 shows the plot of pedal force versus pedal displacement that occurred in the computer simulation, with $K_p = 4$. Interestingly, System A clearly shows that the pedal force associated with maximum pedal displacement was exceeded. The segment described as cable stretch in the

figure denote these force exceedances. Cable stretch means the control cables would likely be stretched when forces exceeding those required for maximum control surface deflection are employed by the pilot. In an actual mechanical flight control system, some pedal motion would be associated with this cable stretch. That is, the segments denoted as cable stretch would not be vertical, but would, instead, have large slopes consistent with large forces, resulting in relatively small pedal motion. Again, it is worth emphasizing that the maximum attainable control surface deflections for both Systems A and B are identical.

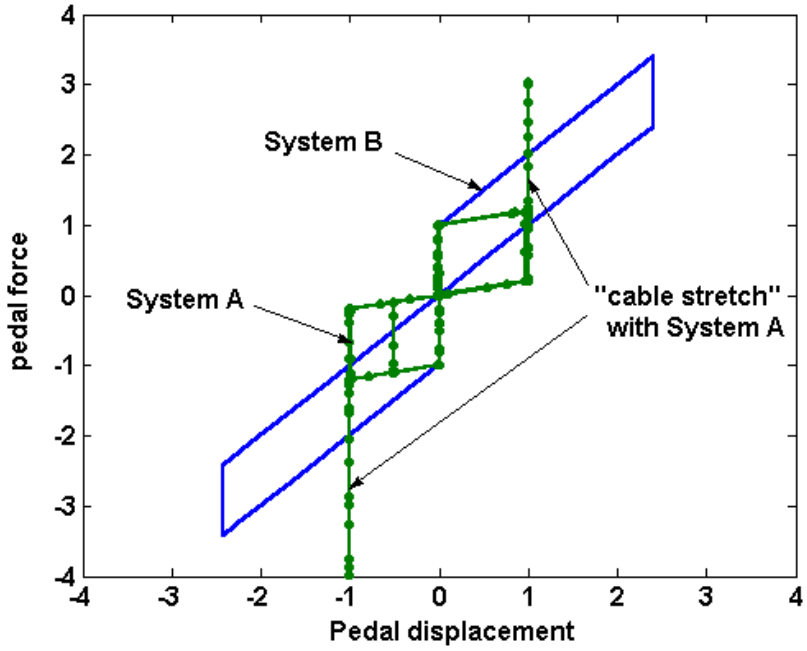

FIGURE 57. PEDAL FORCE VS PEDAL DISPLACEMENT FOR SYSTEMS A AND B IN FIGURE 53 FOR $K_p = 4$

In comparing the results of the computer simulation, it must be emphasized that the two simulations have employed

- identical vehicle models.
- identical forms for the pilot models.
- identical pilot model gains.
- identical maximum control power.
- identical command inputs.

The nature of the vehicle responses were, however, very different. This fact can be attributed solely to the different force/feel systems that were modeled. In other words, in terms of a closed-loop feedback structure that defines human pilot tracking behavior, there is a price to be paid for highly nonlinear force/feel characteristics. Such characteristics can and will produce unpredictable and unsatisfactory response characteristics in closed-loop control.

As previously stated, the primary difference between the two force/feel systems that were modeled is their linearity, or lack of it. A simple way to quantify this property is shown in figure 58.

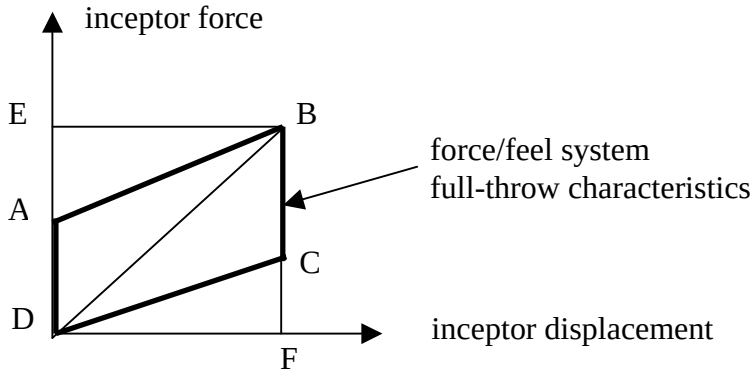

FIGURE 58. DEFINING A LINEARITY INDEX

The heavy lines in figure 58 represent the full-throw force/feel characteristics for the inceptor in question. Line DB was drawn from the origin of the force/displacement graph to the point farthest from the origin. Based on figure 58, one can propose a nondimensional linearity index (LI) as

$$LI = 1 - \frac{Area(DABD) + Area(DBCD)}{Area(DEBFD)} \tag{22}$$

Thus, if LI = 1 in equation 22, the force/feel system is completely linear. If LI = 0, the system could be called completely nonlinear. The simple formula above can easily be extended to force/feel graphs defined by curves rather than straight-line segments. Using the metric above, the LI's for the force/feel systems defined as System A and System B compare as follows:

- System A—LI ≅ 0.14
- System B—LI ≅ 0.76

System B is a factor of 5.4 more linear than System A using LI.

It is useful to note, that for any force/feel system, once a satisfactory breakout force has been determined, the selection of the sensitivity of the system (or its reciprocal, the force gradient) can be based entirely on the value of LI.

Obviously one can create an inceptor force/feel system with a high LI value, but it will prove unacceptable in use. This might involve inceptor force/feel characteristics with no breakout and with a range of applied forces that is far too small (or too large) for the particular human muscle group that is intended to create the forces with any accuracy. Thus, any criterion that might be developed based on some minimum value of LI should be regarded as a necessary, but not a sufficient, condition for the acceptability of the force/feel system. It would appear that small LI

values should almost always be avoided in inceptors that can be used in closed-loop tracking by the human pilot. A low LI value almost invariably indicates an overly sensitive force/feel system in which the breakout and maximum inceptor forces are not sufficiently separated in magnitude.

A final variation in calculating the LI should be discussed. This might apply to a force/feel design in which inceptor forces beyond that associated with maximum control surface deflections are permitted, including allowing proportional pedal motion, but not allowing the larger control surface deflection associated with this increased pedal motion. Essentially, beyond a certain point, pedal motion would not be reflected in control surface motion. The force/feel characteristics for such a system might be represented as in shown in figure 59.

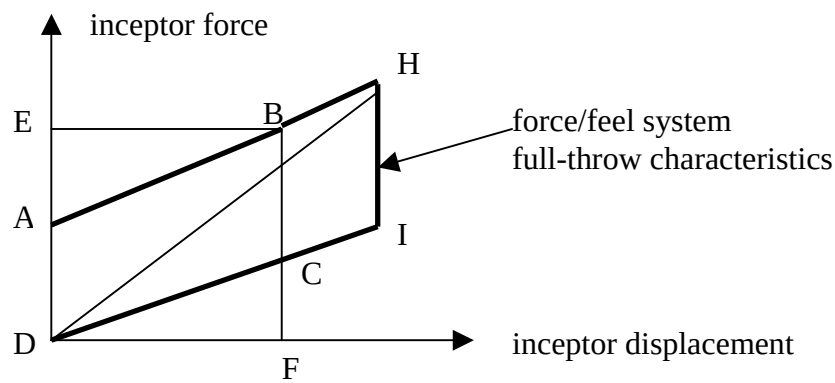

FIGURE 59. ALTERNATE DEFINITION OF LINEARITY INDEX

In figure 59, the line segments BHIC represent that portion of the force/feel trajectory in which inceptor force and position result in no control surface movement. In this case, LI should be defined as

$$LI = 1 - \frac{AREA(DAHD) + AREA(DHID)}{AREA(DEBF)} \tag{23}$$

That is, the normalizing area in the calculation of LI is just that associated with the inceptor force/displacement graph that produces control surface motion. Cases involving possible cable stretch should be treated as if no cable stretch were possible.

3.5 SUMMARY OF SECTION 3.

The research discussed in this section involved a limited comparison of existing pedal force/feel systems in three transport aircraft and an operational military helicopter. The helicopter was included since its pedal force/feel system has been shown to allow precise heading/yaw control. In comparing the pedal force/feel systems for three transport aircraft and a helicopter, the system for one transport was shown to be significantly more nonlinear than that for the remaining three vehicles. A simple computer simulation of a closed-loop piloting task involving two of the force/feel systems differing most in linearity was conducted. It was shown that the highly nonlinear force/feel design led to unpredictable vehicle responses and poor performance. A

linearity index was defined to allow a quantitative comparison of the linearity of force/feel systems.

4. SUMMARY OF RESULTS.

- The handling qualities and flight safety implications of high-gain, closed-loop tracking using coordinated aileron and rudder inputs that were suggested in the analysis were reflected in the desktop simulation.

- Transient use of rudder inputs, i.e., not relying on continuous closed-loop tracking using this control effector, resulted in improved performance in a large roll attitude task compared to when a continuous, closed-loop rudder control was employed.

- The wings-level sideslip capture task, suggested in the analysis as a useful maneuver to investigate handling quality issues, was also supported by the limited desktop simulation study. Large rudder system sensitivity led to an inability to complete the sideslip capture task in the desktop simulation study and further supported the use of this task in a more realistic flight simulation to investigate rudder sensitivity issues.

- The pedal force/feel systems for a helicopter (UH-60A) and two transport aircraft (Boeing 767 and Airbus A300-B2-B4) were compared and found to be significantly more linear in their force/displacement graphs, than that of a third comparison transport (A300-600). The UH-60A was included in the comparison since its pedal force/feel system was shown to allow precise yaw/heading control in demanding handling quality-related maneuvers.

- A simple computer simulation modeling a piloted, closed-loop tracking task clearly demonstrated that highly nonlinear force/feel systems produce poor response predictability and tracking performance compared to more linear force/feel designs.

- A simple linearity index that can vary between zero and unity in value can be used to quantify the linearity of force/feel systems. Force/feel systems with small linearity index values will almost invariably be very sensitive, i.e., will exhibit a small difference between breakout and maximum forces applied to the inceptor.

5. CONCLUSIONS.

An analytical and limited experimental study was conducted to investigate the handling qualities and flight safety implications of rudder control strategies and systems in transport aircraft. The study focused on the dynamics of a single representative transport aircraft, a dynamic model of which is readily available in the literature. The preliminary and simplified nature of this study must obviously be borne in mind in interpreting the conclusions that follow. In addition, a limited comparison of existing force/feel characteristics of four aircraft was undertaken. Based on this study, the following conclusions can be drawn.

- A system survey of possible manual loop closure that could be employed by the pilot, using rudder control, led to an examination of two tracking strategies that could occur in large roll upsets and deliberate sideslip excursions. These strategies were the coordinated use of aileron and rudder inputs and wings-level sideslip captures.

- Using bandwidth and phase delay measures, the coordinated use of aileron and rudder inputs was predicted to result in low obtainable bandwidths in roll attitude control. Although no bandwidth boundaries were established for acceptable handling qualities in tasks involving coordinated use of aileron and rudder, the relatively small bandwidth values suggest poor handling qualities in such tasks in anything, save low-bandwidth operations.

- The analysis suggested that rudder force/feel systems with large sensitivities (or equivalently, low-force gradients) could precipitate pilot-induced oscillations when a coordinated use of ailerons and rudder was employed. This susceptibility could be attributed to large lateral accelerations occurring at the pilot's station.

- The analysis suggested that wings-level sideslip captures might serve as a useful pilot-in-the-loop flight simulation task to investigate handling quality issues involving rudder control.

6. REFERENCES.

1. Dornheim, M.A., "Did Rudder Motions Snap Off A300 Fin?" *Aviation Week and Space Technology,* January 21, 2002, pp. 24-26.

2. Dornheim, M.A., "Crash Probe Triggers Rudder Design Scrutiny," *Aviation Week and Space Technology,* April 1, 2002, pp. 44-46.

3. Dornheim, M.A., "Flight 587 Probe Shows Tails Have Been Overloaded Before," *Aviation Week and Space Technology,* November 25, 2002, pp. 44, 49-51.

4. Fiorino, Frances, "Upset Events, Wake Vortices at Center of Flight 587 Probe," *Aviation Week and Space Technology,* April 22, 2002, p. 39.

5. McRuer, D., Ashkenas, I., and Graham, D., *Aircraft Dynamics and Automatic Control,* Princeton University Press, Princeton, NJ, 1973, chapter 8.

6. Stapleford, R.L., McRuer, D.T., and Magdaleno, R.E., "Pilot Describing Function Measurements in a Multiloop Task," *IEEE Transactions on Human Factors in Electronics,* Vol. HFE-8, No. 2, June 1967, pp. 113-124.

7. Mitchell, D.G., Hoh, R.H., Aponso, B.L., and Klyde, D.H., "Proposed Incorporation of Mission-Oriented Flying Qualities into MIL-STD-1797A," WL-TR-94-3162, Wright Laboratory, Wright Patterson AFB, OH, October 1994.

8. Preston, J.D., et al., "Unified Pilot-Induced Oscillation Theory, Vol. II, Pilot-Induced Oscillation Criteria Applied to Several McDonnell Douglas Aircraft," WL-TF-96-3029, Wright Laboratory, Wright-Patterson AFB, OH, December 1995.

9. Hess, R.A., "Feedback Control Models—Manual Control and Tracking," *Handbook of Human Factors and Ergonomics,* G. Salvendy, ed., Wiley, New York, 1997, chapter 38.

10. Hess, R.A., "Unified Theory for Aircraft Handling Qualities and Adverse Aircraft-Pilot Coupling," *Journal of Guidance, Control, and Dynamics,* Vol. 20, No. 6, November-December 1997, pp. 1141-1148.

11. Hess, R. A., "An Inquiry Into Whether a Pilot-Induced Oscillation was a Factor in the Crash of American Airlines Flight 587," a report submitted to the National Transportation Safety Board, January 2003.

12. Graham, D. and McRuer, D., *Analysis of Nonlinear Control Systems,* Dover, New York, 1961, p. 228.

13. Gibson, J.C. and Hess, R.A., "Stick and Feel System Design," AGARDograph 332, March 1997.

14. Anon., "STEADES—Safety Trend Evaluation, Analysis & Data Exchange System," first interim report, December 20, 2002, Transport Category Airplane Rudder and Lateral Control Events, International Air Transport Association (IATA).

15. Anon., *Aviation Safety and Pilot Control—Understanding and Preventing Unfavorable Pilot-Vehicle Interactions,* National Academy Press, Washington, DC, 1997, chapter 5.

16. Smith, R.H., "Quick Start Manual for HPESIM," HPE-MAN-QSSIM-0.1.01, High Plains Engineering, 1999.

17. Anon., "Aeronautical Design Standard, Performance Specification Handling Qualities Requirements for Military Rotorcraft," ADS-33E-PRF, U.S. Army Aviation and Missile Command, March 2000.

18. Heffley, R.K., Hess, R.A., and Zeyada, Y., "Computer Modeling and Simulation for Helicopter Pilotage Task Analysis," U.S. Army Aviation and Missile Command, Research, Development & Engineering Center, USAAMCOM TR 02-D16, June 2002.